



# Accuracy evaluation of a new generic Trajectory Prediction model for Unmanned Aerial Vehicles



Mingyang Huang <sup>a,\*</sup>, Washington Yotto Ochieng <sup>a</sup>, Jose Javier Escribano Macias <sup>a</sup>, Yi Ding <sup>b,c</sup>

<sup>a</sup> Centre for Transport Studies, Imperial College London, Exhibition Road, London SW7 2AZ, UK

<sup>b</sup> Airbus, Toulouse 31703, France

<sup>c</sup> ISAE-SUPAERO, Université de Toulouse, Toulouse 31055, France

## ARTICLE INFO

### Article history:

Received 19 March 2021

Received in revised form 20 September 2021

Accepted 30 September 2021

Available online 11 October 2021

Communicated by Xingqun Zhan

### Keywords:

Unmanned Aerial Vehicle

Trajectory Prediction

Accuracy

Error budget

Validation

## ABSTRACT

Unmanned Aerial Vehicles (UAVs) attract much attention, and they require trajectory information for planning and tactical operations. Based on the current trajectory data obtained by navigation systems, appropriate Trajectory Prediction (TP) models are required to determine future UAV trajectories. Regardless of the disparity of the models, the knowledge of TP accuracy and its performance evaluation are of paramount importance. After the review of extensive literature on current TP models, this paper develops a more accurate TP model by creating valid methodologies for error budgeting and mitigation. This is followed by the specification for quantifying TP accuracy and sub-functional testing employed in the process of model development. The new model is tested and validated by three credible case studies in relation to the most stringent UAV applications. The validation evidence demonstrates that the new model improves TP accuracy based on previous models.

© 2021 Elsevier Masson SAS. All rights reserved.

## 1. Introduction

Scientific advances in aerospace technologies have enabled a wide range of aircraft operations. Unmanned Aerial Vehicles (UAVs) are a new type of aircraft without a pilot on-board, controlled either remotely or autonomously [1]. There has been a steadily growing market for UAVs [2], with their potential socio-economic benefits (e.g., reducing air accidents, stimulating economic growth, improving service provisions) being clear and substantial. All UAV operations require description and representation of their movements through space and time in terms of location, time, and derivative information for planning and tactical operations. This information constitutes the trajectory of a UAV, and the requirement for such information calls for the capability to predict trajectories. Trajectory Prediction (TP) is defined as the forecast of the future path as a function of time. Supported by TP capabilities, UAV operations benefit from both direct and indirect information. The latter involves control of relevant on-board sensors for proximate obstacle detection and avoidance [3].

Each UAV operation has user-level requirements: localisation accuracy [4], safety [5], punctuality and timeliness [6]. To fulfil such requirements related to location, trajectory, and schedule data, Positioning, Navigation, and Timing (PNT) technologies are required [7]. PNT requirements are expressed in terms of the Required Navigation Performance (RNP) which is on the accuracy basis [8]. Accuracy is the degree of conformance of an expected position with the true position. Based on the current trajectories obtained through PNT technologies, TP models are required to determine future trajectories. To keep the deviation between the predicted and planned trajectories to a minimum, TP performance should be the same in statistical terms as RNP (on the accuracy basis).

In order to generate accurate and realistic UAV trajectories, TP requires information about initial states, weather and UAV performance to properly model UAV intents and motions. Previous TP models [9] have developed some of these parts: the estimation of initial states, the modelling of motions, the knowledge of UAV performance, the inference of intents, and the forecast of weather conditions. However, current TP models only consider individual error sources in limited cases, and the other TP errors are forwardly propagated throughout the TP process.

\* Corresponding author.

E-mail address: [m.huang18@imperial.ac.uk](mailto:m.huang18@imperial.ac.uk) (M. Huang).

UAV initial states strongly influence TP accuracy, because they are the inputs of TP models. To mitigate the initial state errors, multi-sensors are integrated to replace the sole means of navigation, because their benefits and drawbacks are complementary [8]. To estimate the UAV initial mass, an energy-rated model involves deterministic methods based on the total aircraft energy [10]; however, this model has inherent errors because of the simplification of the aircraft operating scene. Recently, the mass estimation problem has been considered as a single parameter Bayesian inference problem [11]. The Bayesian inference method incorporates non-linear evolution equations for the nonlinear Bayesian filtering of the aircraft mass [12], which will be considered in this paper.

The modelling of aircraft motions was simplified by a point mass model [12], which leads to aircraft performance errors. Some TP models assess aircraft performance by using the data acquired during real flight trials; however, some UAV flight data are inaccessible. UAV performance was analysed by machine learning methods [13] based on its speed [14]; however, the observed values of the UAV speed have uncertainties, which further increase TP errors. To mitigate aircraft intent errors, a TP model uses trajectory conformance monitoring as a trigger [15]; however, it is not suitable for multi-rotor UAVs. Previous TP models propose time lagged ensembles to characterise the weather forecast error [9], which will be considered in this paper to improve TP accuracy.

On the basis of the accurate TP, the optimal (i.e., safest and shortest) trajectories can be determined by considering the constraints [16]. To handle the constrained TP problem, an approximation-based strategy uses a smooth and differentiable function to replace probabilistic constraints by the deterministic ones [17]. A trajectory optimisation model includes pitch angle, curvature radius, and collision avoidance constraints [18], which will be considered in this paper. In recent years, there is a growing trend of designing artificial intelligence schemes [19] to meet the demand for better TP performance. A deep neural network-based scheme was developed for the TP in taxiing phases [20], and a bilevel structure incorporating deep neural network-based control was used for flight path planning [21]. The artificial intelligence schemes unavoidably include black boxes instead of specifying vehicle dynamics in the modelling process. This paper mainly considers model-driven methods to specify the details of the TP model and its inter-relationship.

In summary, a number of TP models have been improved to support a wide range of applications; however, the research to date on TP for UAV operations has three limitations, which negatively impact TP accuracy [22]. First, previous TP models involve a set of assumptions which simplify the relationship between the UAV and its Vehicle Dynamic Model (VDM) [23]. Secondly, current TP models are very limited focusing on a subset of UAV applications [24] instead of responding to all the applications. Thirdly, current TP models have not been verified in each phase of a flight profile [25], with the consequence that these models will be not generically applicable.

To address these limitations, this paper aims to mitigate TP errors and develop a generic TP model applicable to different UAV applications. It starts with the establishment of a high-level functional architecture of the TP model in Section 2. This is followed by the quantitative modelling of each error component in a UAV full-state model and error budgeting in Section 3. To address each error component, this paper incorporates new error modelling techniques in Section 4. To validate the performance of the TP model in different flight phases and UAV applications, three credible case studies are specified and implemented, and then their results are analysed in Section 5.

## 2. Functional architecture of Trajectory Prediction model

All UAV applications require description of UAV operations in terms of location-based information. For instance, UAV deliveries require localisation services to support self-localisation and in return localise obstacles. In this paper, mission control and end-user location-based information are treated together and are referred to as Location Based Services (LBS) [26]. In the delivery of LBS, a key prerequisite is the capability to guarantee common Situational Awareness (SA) amongst relevant stakeholders, which is the spatial recognition of the physical environment surrounding UAVs. To accurately recover the real proximate environment at the time of SA, a TP model is required for the prediction of the full states of relevant on-board sensors. Within the projection function of SA, TP models are required to predict future UAV states before and during the flight.

Based on SA and taking account of stakeholder requirements, path planning and execution are required for UAV operations. The former generates consistent collision-free paths from origin to destination in the physical environment [27]; thus, TP models are required to improve prior strategic predictions to ensure safety in flight. Path execution navigates the UAVs along their planned paths to ensure that the deviation between the actual and planned paths is within a pre-defined tolerance. To support the navigation and other functions in path execution, TP models are required. In order to keep the deviation between the planned and executed paths to a minimum, it is important to examine the PNT requirements for the relevant LBS. The achievement of the PNT requirements ensures that each LBS is delivered in the most efficient manner to achieve the required capacity, safety, cost-effectiveness, and environmental impact. Therefore, TP performance should aim to be the same in statistical terms as the PNT requirements.

Path execution aims to ensure that the actual path is in conformance with the planned path; thus, its metrics should cover trajectory conformant requirements, which are related to accuracy. To determine the level of conformance (i.e., accuracy), a tactical TP model is required to predict the actual path in the short term in the form of a time-ordered set of spatial data. If the deviation between the predicted and planned paths exceeds the accuracy requirement which is a pre-defined tolerance, trajectory adjustment and attitude control functions are required to change the UAV movement to reduce the deviation, ensuring a conflict free (from proximate UAVs and other physical obstacles) flight.

The functional architecture of the TP model starts with input data, followed by a comprehensive description of the UAV TP process and its output solutions. The functional architecture of the TP model includes different fundamental elements as follows.

- Metrics for TP performance measurement and evaluation purposes.
- Operational conditions under which the TP performance is measured and evaluated.
- Factors that lead to TP errors.
- Components of TP models.
- Application for the demonstration of TP models.

To underpin UAV operations, the functional architecture of the TP model is shown in Fig. 1.

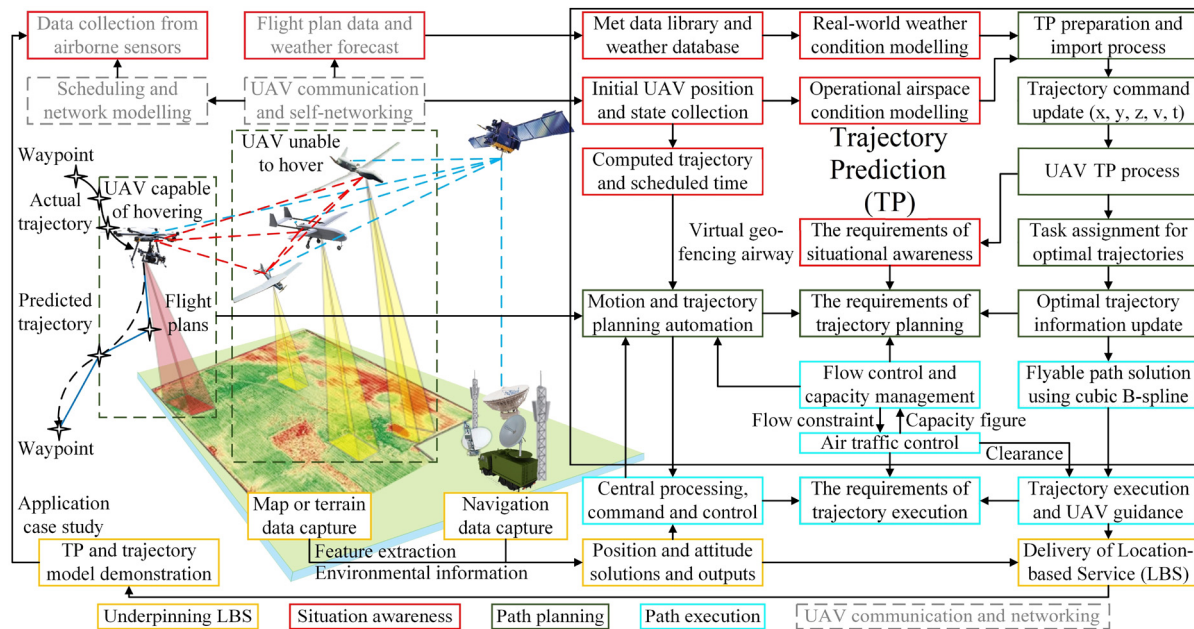


Fig. 1. A functional architecture of the TP model.

### 3. Trajectory Prediction error budgeting in a full-state model

Currently, there is a huge variety of TP implementations that support a wide range of location-based applications. Regardless of the disparity of TP implementations, TP accuracy, which is the fundamental requirement for the implementation, is the essential parameter to be determined; thus, the evaluation of TP accuracy is of paramount importance.

A TP process encompasses five parts: initial state estimation, intent inference, weather forecast, trajectory modelling, and performance modelling. To improve TP accuracy, previous models mitigate errors in different parts of the TP process. This section budgets the total TP error by reviewing the best error mitigation methods to date for each part.

#### 3.1. Trajectory Prediction error components in a full-state model

TP accuracy reflects the capability to precisely predict UAV full states (e.g., longitude, latitude, altitude, pitch, roll, yaw) with respect to the actual states sampled over the same flight phase. Without accurate UAV full-states, TP accuracy might exceed the upper limit and become unacceptable after a short term. TP accuracy is referred to as the total error, consisting of a Navigation System Error (NSE), a Path Definition Error (PDE), and an Autonomous Flight Error (AFE).

- The NSE reflects the performance of the navigation system in practice, and it leads to the state error at the beginning of each flight phase, which is referred to as the initial state error.
- The PDE is caused by the lack of fidelity of the model. The PDE is influenced by intent update and trajectory modelling errors, which require further analysis in the following sections.
- The AFE reflects the flight mistake affected by the UAV performance error and wind bias; thus, accurate performance and wind forecast models are required to ensure a tolerable AFE.

#### 3.2. Trajectory Prediction error budgeting

The total error budget considers the best error mitigation methods to date for each part of TP.

- **Initial state error:** A typical set of initial state data comprises the initial time, position, location, velocity, acceleration, attitude, and mass. This paper assumes that the navigation system time is perfectly synchronised with the satellite clock time, and Global Navigation Satellite System (GNSS), Inertial Navigation System (INS), radar, Light Detection and Ranging (LiDAR) are integrated to deliver centimetre-level positioning; thus, the initial time and position errors are mitigated to 0 s and 1 cm. A number of relatively new navigation systems, which include Wireless Local Area Network (WLAN), Ultra-Wideband Technology (UWB), Bluetooth, and 5th-Generation (5G) wireless systems, are used to mitigate location and velocity errors [28]. To avoid acceleration and attitude errors being forwardly propagated throughout the computation process, the GNSS and INS are integrated to offer a continuous, high-bandwidth, and complete navigation solution with high long-term accuracy. GNSS measurements prevent the inertial solution drifting, and the INS can smooth the GNSS solution and bridge signal outages. To infer the varied UAV mass, an accurate Bayesian inference method incorporates non-linear evolution equations; however, it yields a mean absolute error of 4.3% of the true mass [12]. Accordingly, the Bayesian inference method additionally leads to 4.3% of UAV initial state errors.
- **Trajectory modelling error:** Previous trajectory models, available in the open literature, make a number of assumptions [9] to simplify the mathematical formulations of aircraft motions. This simplification neglects the deflections of aerodynamic control surfaces and leads to aerodynamic force errors. According to such models, the modelling intrinsic error is related to the UAV speed, and it is

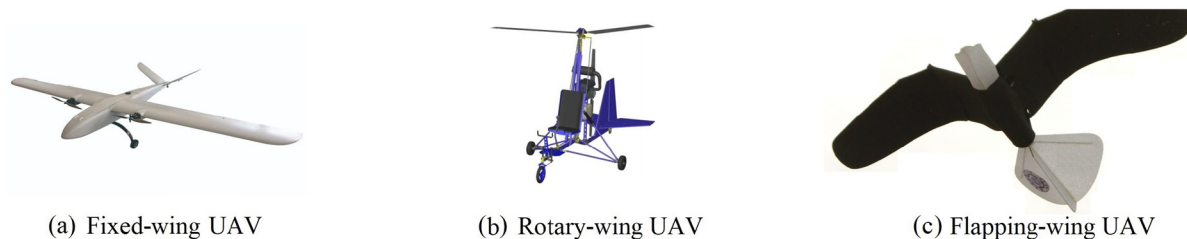


**Fig. 2.** HTOL UAVs including fixed-wing, rotary-wing, and flapping-wing UAVs.

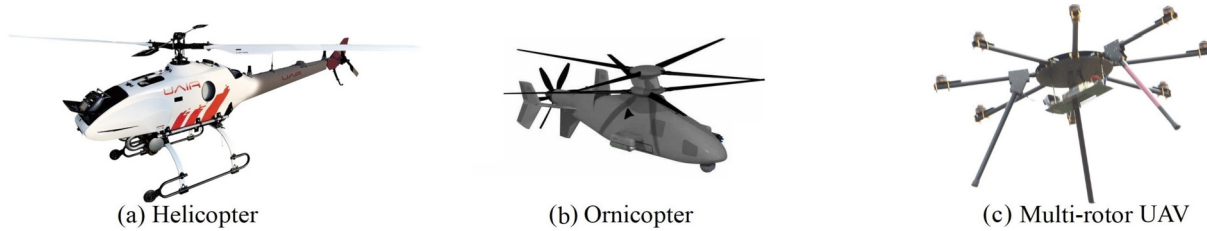


**Fig. 3.** VTOL UAVs including unmanned helicopter, ornicopter, and multi-rotor UAVs.



**Fig. 4.** Hybrid UAVs including tilt-fuselage UAVs, tilt-wing UAVs, and tilt-rotor UAVs [30].

around the flight distance during 8 s. To mitigate this error, a set of differential algebraic equations are required to integrate the diverse trajectories of different UAVs to accurately describe UAV motions. Some motion problems have no analytical solution; thus, a numerical method is required to output a numerical solution that approximates its corresponding analytical solution (which might be non-existent). By adopting a small interpolation interval, the deviation between the numerical and analytical solutions can be mitigated to be less than 1 cm.

- **Vehicle performance errors** pose a great challenge to TP due to the lack of aerodynamic data. In manned aviation, manufacturers provide aerodynamic performance based on numerous wind tunnel tests. Considering the rapid growth of UAV markets, the low manufacturing costs, and the short manufacturing cycles of UAVs [29], the manufacturers do not follow the traditional way in manned aviation to conduct enough tests. Some UAV manufacturers are unwilling to share aerodynamic data which belong to intellectual properties; thus, this paper applies the quasi-steady method to calculate the aerodynamic force and UAV propeller/rotor thrust. The latter is different from the combustion turbine engine force of fixed-wing commercial aircraft.
- **Intent update errors** are directly related to flight modes, speeds and durations. In terms of their flight modes, all UAVs are classified into three types: Horizontal Take-off and Landing (HTOL) UAVs, Vertical Take-off and Landing (VTOL) UAVs, and hybrid UAVs. HTOL UAVs have the same intent update error characteristics as fixed-wing commercial aircraft, for which a standard deviation of 10000 m (equivalent to the flight distance during 40 s) is used to characterise the intent update error [15]. This error is mitigated by using a trajectory conformance monitor as a trigger, and the residual discrepancy between the actual and planned paths is less than 1500 m (equivalent to the flight distance during 6 s) at each waypoint. For HTOL UAVs, the flight distances during 40 s and 6 s are set to be their intent update errors before and after error mitigation. VTOL and hybrid UAVs are able to hover in the air and have enough time for intent adjustment; thus, their intent update errors can be reduced to zero after hovering for error correction. See Figs. 2–4.
- **Weather forecast error:** The most sophisticated weather models use assimilation techniques to introduce actual weather data, leading to a position error of less than 2 m [9]. Previous wind forecast models propose time lagged ensemble methods to characterise the wind bias, which are sufficient for UAV TP; thus, they are utilised in the TP model in this paper.

After the review of previous TP models and error modelling techniques, the error sources and error budgeting are consolidated into an exhaustive list in Table 1.

**Table 1**  
The error sources of TP accuracy and error budgeting.

Error category	Error type (Leading to state error)	Error-caused state deviation description	Actual UAV state deviation magnitude	The best error mitigation method	Residual magnitude of error after mitigation
Initial state error	Initial time error (Leading to UAV position, speed, and attitude errors)	The position or trajectory deviation caused by the error of the initial local time obtained by satellite navigation systems	Position error 5-10 m Speed error 0.012 m/s Attitude error 0.003 rad	Assume that UAVs have along-track movements during the time intervals to transform time errors into position errors [7]	Position error 0 cm Speed error 0 m/s Attitude error 0 rad
	Initial position error (Leading to UAV position and speed errors)	The deviation between the actual and predicted initial latitude/longitude/altitude referenced to the Earth caused by satellite, atmosphere, receiver, or transmission errors	Latitude error 5-10 m, longitude error 5-10 m, altitude error 10-20 m Speed error 0.2 m/s	Use differential GNSS and infrastructure (e.g., on-board reference unit, reference station, local base station) to improve the satellite navigation accuracy [28]	Latitude error 2 cm, longitude error 2 cm, altitude error 3 cm Speed error 0.1 cm/s
	Initial location error (Leading to UAV position, location, speed, and attitude errors)	The deviation between the actual and predicted locations referenced to another object caused by the errors of the WLAN, barometric altimeter, radar, LiDAR, 5G, and other navigation systems	Latitude error 40.3 m, longitude error 40.2 m, altitude error 53.6 m Horizontal error 5-10 m, vertical error 10-20 m Speed error 0.2 m/s Attitude error 0.003 rad	Integrate the WLAN, barometric altimeter, radar altimeter, LiDAR, 5G, and other navigation technologies to improve the navigation accuracy [28]	Latitude error 1.8 cm, longitude error 1.65 cm, altitude error 2.82 cm Horizontal error 1-2 cm, vertical error 2-4 cm Speed error 0.1 cm/s Attitude error 0.00003 rad
	Initial velocity error (Leading to UAV position and speed errors)	The deviation between the actual and predicted values of the magnitude of the basic velocity	Position error 5-10 m Along-track speed error 1.5 m/s, cross-track speed error 0.6 m/s	Utilize the on-board air pressure transducers and amplifier circuits to mitigate speed errors	Position error 1-2 cm Along-track speed error 0.1 m/s, cross-track speed error 0.03 m/s
	Initial acceleration error (Leading to UAV position, speed, and acceleration errors)	The deviation between the actual and predicted values of the magnitude of acceleration caused by inertial navigation errors	Position error 15 km (after 30 minutes) Speed error 0.6 m/s Acceleration error 0.1 m/s <sup>2</sup>	Integrate INS and GNSS measurements to prevent the error propagation [28]	Position error 500-1300 ppm Speed error 0.02 m/s Acceleration error 0.003 m/s <sup>2</sup>
	Initial attitude error (Leading to UAV attitude errors)	The deviation between the actual and predicted values of the attitude of each UAV referenced to Earth or another object caused by INS errors	Pitch angle error 0.18 rad, yaw and roll angle errors 0.35 rad	Combine INS and GNSS technologies to offer a new continuous, high-bandwidth, and complete navigation solution with high long-term accuracy	Pitch angle error 0.015 rad, yaw and roll angle errors 0.029 rad
	Initial mass error (Leading to UAV position, speed, and acceleration errors)	The deviation between the actual and predicted values of UAV states caused by the mass error	Additional 30% of the position, speed, and acceleration errors	Use Bayesian inference methods for the Bayesian filtering of the UAV initial mass [12]	Additional 4.3% of the position, speed, and acceleration errors
	Intent update error of HTOL UAVs	The variation on the actual maneuver of each UAV compared to the trajectory	Flight distance during 40 s	Utilize the trajectory conformance monitoring as a trigger to correct intent update errors [15]	Flight distance during 6 s
	Intent update error of VTOL and hybrid UAVs	that is predicted based on the initial intent of the UAV	Flight distance during 40 s	Maintain UAV real-time positions to adjust intents during hovering [30]	0 m

(continued on next page)

Error category	Error type (Leading to state error)	Error-caused state deviation description	Actual UAV state deviation magnitude	The best error mitigation method	Residual magnitude of error after mitigation
Trajectory modelling error	Trajectory modelling intrinsic error (Leading to UAV position error)	The position deviation caused by assumptions considered to define UAV motion models	The deviation between the actual and computed trajectories	Utilize a mathematically solvable system to predict the successive UAV trajectories [9]	Flight distance during 8 s
	Solvability error (Leading to UAV position error)	The position or trajectory deviation caused by the numerical methods that are selected for obtaining solvable systems	The deviation between the numerical solution and its analytical solution that might be non-existent	Combine the numerical methods (approximation methods) with the UAV motion models to output numerical solutions [9]	Position error 1 cm
UAV performance error	Aerodynamic error (Leading to UAV position, speed, and acceleration errors)	The deviations between the actual and predicted states caused by the error of aerodynamic forces	Additional 6% of the position, speed, and acceleration errors	Adjust real-time flight data to better fit the actual performance [29]	Additional 1.5% of the position, speed, and acceleration errors
	Propulsion error (Leading to UAV position, speed, and acceleration errors)	The deviations between the actual and predicted values of the UAV states caused by the thrust error	Additional 24% of the position, speed, and acceleration errors	Build accurate engine performance degradation models to evaluate the propulsion loss [29]	Additional 6% of the position, speed, and acceleration errors
	Operational limitation-derived error (Leading to UAV position error)	The difference between the actual trajectory and on-board reference due to operational limitations	The deviation between the actual path and its on-board reference	Consider the error as the external noise acting on the nominal TP [9]	0 m
Weather forecast error	Atmosphere forecast error (Leading to UAV position error)	The position or trajectory deviation caused by the temperature, air density, and pressure condition forecast errors at a given time and location	Position error 350 m	Make use of assimilation techniques to introduce the actual atmosphere data in the initialization process [9]	Position error 2 m
	Wind forecast error (Leading to UAV position and speed errors)	The deviation between the actual and predicted values of the UAV states caused by wind forecast errors at a given time and location	Position error 750 m Speed error 20 m/s	Make use of assimilation techniques and utilize the quasi-steady method for spatial-temporal wind error calculation [9]	Position error 0 (indoor), 7.5 m (urban space in Wellington), 15 m (suburban space, twice as much as urban space), or 50 m (airspace) [9] Speed error 2.5 m/s

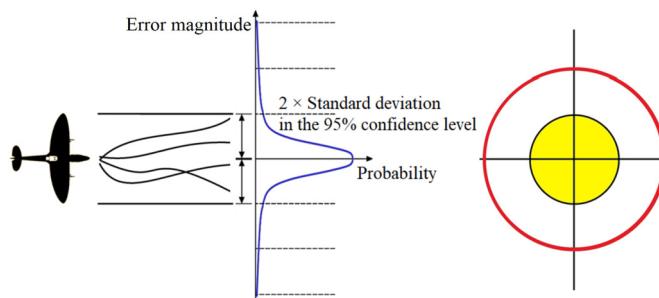


**Fig. 5.** The error distribution in normal condition (i.e., Gaussian distribution).

The intent update and trajectory modelling errors are related to the UAV speed, and their combination can be represented by the UAV flight distance during an operation time period.

**Intent update errors:** For UAVs unable to hover, their intent update errors are unavoidable and unneglectable because of their specific flight capabilities and performance (i.e., relatively high-speed movement, highly dynamic operation, and unable to hover). UAVs unable to hover have the same intent update error characteristics as fixed-wing commercial aircraft. Previous 4-D TP methods [15] utilised trajectory conformance monitoring to generate new intents, and the intent update error is mitigated to 1500 m (equivalent to the flight distance during 6 s, because the flight speed is 250 m/s); thus, the flight distance during 6 s is set to be the intent update error residual. UAVs capable of hovering have enough time to reduce their intent update errors to zero after hovering.

**Trajectory modelling errors:** According to the trajectory models to date [9], for each UAV, the flight distance during 8 s is set to be its trajectory modelling error residual.

**Combination of errors:** For the UAV unable to hover, the flight distance during 6 s is set to be its intent update error; thus, the total residual of the intent update and trajectory modelling errors of the UAV unable to hover is represented by the UAV flight distance during a given time interval (i.e.,  $\sqrt{(8^2 + 6^2)} \text{ s} = 10 \text{ s}$ ). The UAV capable of hovering can maintain its real-time position to correct its intent update error; thus, its intent update error can be reduced to zero after hovering, and the total residual of the intent update and trajectory modelling errors is represented by the UAV flight distance during 8 s. In summary, the total residual of the intent update and trajectory modelling errors of each UAV depends on the UAV flight distance during a certain operation time period (i.e., "8s" for VTOL UAVs and hybrid UAVs capable of hovering, and "10s" for HTOL UAVs unable to hover).

TP accuracy is expressed as the total error, which is addressed with respect to all error sources. The total error is expressed as a function of the initial state error, intent update error, trajectory modelling error, UAV performance error, and weather forecast error in Equation (1).

$$\text{Total error} = \zeta \text{ (Initial state error, Intent error, Modelling error, Performance error, Weather forecast error)} \quad (1)$$

This paper assumes that the actual magnitude of each error component (denoted by |Error component|) is in conformance to the normal behaviour of distribution in Fig. 5.

After the error mitigation, the distribution of the residual of each error component is represented by a Gaussian distribution. These residuals are the components of the total error residual, which can also be represented by a Gaussian distribution. The probability of the actual magnitude of each error component can be expressed as  $\frac{1}{\sqrt{2\pi}\sigma(\text{Error component})} e^{-\left[\frac{|\text{Error component}|^2}{2\sigma(\text{Error component})^2}\right]}$ , where  $e$  represents Euler Number and  $\sigma$  (Error component) represents the standard deviation of the error component after error mitigation. The actual magnitude of each error component needs to be within a specified performance limit (denoted by  $\pm 2\sigma$  (Error component)) for 95% of the operation time; thus,  $4\sigma$  (TP error) represents the residual magnitude of the error component after error mitigation.

The residual magnitudes of the initial time error (0 cm), initial position error (latitude error 2 cm, longitude error 2 cm, altitude error 3 cm), initial location error (horizontal error 2 cm, vertical error 4 cm), initial velocity error (2 cm), initial acceleration error (1300 ppm), and solvability error (1 cm) are less than 5 cm; thus, they are neglected in the calculation of the residual of the total error. The total residual of the intent update and trajectory modelling errors is represented by the UAV flight distance during a given time interval. After error mitigation, the standard deviation of the total error is denoted by  $\sigma$  (Total error). The mathematical model for calculating the residual magnitude of the total error after error mitigation (denoted by  $4\sigma$  (Total error)) is expressed in Equation (2).

$$\text{The residual magnitude of the total error after mitigation} = 4\sigma \text{ (Total error)}$$

$$= 4\sqrt{\sigma(\text{Initial state error})^2 + \sigma(\text{Intent update error})^2 + \sigma(\text{Modelling error})^2 + \sigma(\text{Performance error})^2 + \sigma(\text{Weather forecast error})^2}$$

$$= \begin{cases} 1.118 \times \sqrt{(\text{Flight distance during } 8 \text{ s})^2 + (\text{Wind forecast error})^2 + 4 \text{ m}} & \text{(VTOL and hybrid UAVs capable of hovering)} \\ 1.118 \times \sqrt{(\text{Flight distance during } 10 \text{ s})^2 + (\text{Wind forecast error})^2 + 4 \text{ m}} & \text{(HTOL UAVs unable to hover)} \end{cases} \quad (2)$$

### 3.3. Validation for the error budget

To validate the total error budget, three case studies are built to output the total position errors of all types of UAVs (i.e., HTOL aircraft, hybrid and VTOL UAVs) as follows.

**Table 2**  
The total error budgets of case studies.

Case study number	1	2	3
Aircraft type	HTOL aircraft	Hybrid UAV	VTOL UAV
Operational space	Civil airspace	Urban space	Confined space
Flight speed	200 m/s	6 m/s	0 m/s
Reference error	2500 m	50 m	2 m
Total error budget	2237 m	54.3 m	2.236 m
Conformance or not	Conformance	Conformance	Conformance

In first case study, the operation of fixed-wing aircraft (i.e., a type of HTOL aircraft) is analysed. This case study assumes that the fixed-wing aircraft is operated in an airspace, where the wind forecast error is 50 m. The total residual magnitude of intent update and trajectory modelling errors is expressed as the aircraft flight distance during 10 s. The aircraft speed is set to be 200 m/s; thus, its flight distance during 10 s is set to be 2000 m. According to Equation (2), the total error budget of TP accuracy is 2237 m. For the comparison with the total error budget, the total position error of the same fixed-wing aircraft is reviewed as follows. A constrained-based semantic TP approach was adopted to model the trajectory of the same fixed-wing aircraft to reduce its total position error to be 2500 m [31]. The simulated result is in conformance to the total error budget.

In second case study, the operation of tilt-rotor UAVs (i.e., a type of hybrid UAVs) is analysed. This case study assumes that the tilt-rotor UAV is operated in an urban space, where the wind forecast error is 7.5 m. The total residual magnitude of intent update and trajectory modelling errors is expressed as the UAV flight distance during 8 s. The speed of the tilt-rotor UAV is set to be 6 m/s; thus, the flight distance during 8 s is set to be 48 m. According to Equation (2), the total error budget of TP accuracy is 54.3 m. For the comparison with the total error budget, the total position error of the same tilt-rotor UAV is reviewed as follows. A simulation of the same tilt-rotor UAV was performed in a 700 m × 300 m × 200 m urban space, and the total position error converged below 50 m [32]. The simulated result is in conformance to the total error budget.

In third case study, the operation of multi-rotor UAVs (i.e., a type of VTOL UAVs) is analysed. This case study assumes that the multi-rotor UAV is operated in a confined space, where the wind forecast error is 0 m. The total residual magnitude of intent update and trajectory modelling errors is expressed as the UAV flight distance during 8 s. The VTOL UAV is capable of hovering and maintaining its real-time position; thus, its flight distance during 8 s is 0 m. According to Equation (2), the total error budget of TP accuracy is 2.236 m. To compare with the error budget, the total position error of the same multi-rotor UAV is reviewed as follows. A neural network-based approach was adopted to model the trajectory of the same multi-rotor UAV, and it reduces the position error to be less than 2 m [33]. The simulated result is in conformance to the total error budget.

In these case studies, the test results are in conformance to the error budgets, which validates the error budgeting methods. The error budgets of these case studies are listed in Table 2.

#### 4. Trajectory Prediction model development

To mitigate TP errors, this section develops a new model based on the following assumptions.

- Assumption 1: The difference between the true airspeed (i.e., the actual speed relative to the airmass) and the indicated airspeed (i.e., the measured speed) is negligible.
- Assumption 2: UAVs are able to share their trajectory information to facilitate collision avoidance.
- Assumption 3: UAVs and off-board navigation systems have no systemic problem.
- Assumption 4: When UAVs move on the ground, they only use wheels instead of rotors or propellers which might injure people and properties.
- Assumption 5: Due to the high speeds of fixed-wing UAVs, their fuselage deformations affect the aerodynamic forces applied on the deformed parts. The UAV fuselage carries system modules and payloads; thus, it has no common aerodynamic configuration, and there is no generic model that represents its deformation. The UAV fuselage is considered as rigid solid without structural flexibility; thus, all the points of the fuselage maintain their relative positions at all the time.
- Assumption 6: The UAV and payloads have constant mass distributions; thus, the location of the UAV centre-of-gravity is fixed, and the ratio of moment of inertia to mass is constant.

TP can be carried out on strategic and tactical levels, which are tackled by different technologies. Strategic TP represents a forecast from a macroscopic view (hours to a day) before departure based on flight plans, schedules, intents, static data, and weather information, which are known in advance. Tactical TP represents a forecast in a short period (seconds to minutes) for detecting immediate risk of conflicts and collisions based on the latest tactical clearances and VDMs.

##### 4.1. Strategic Trajectory Prediction model development

Strategic TP is mainly applied on the UAV with a specific flight plan, in order to move the UAV from origin to destination safely. The basic principles of the strategic TP are listed as follows.

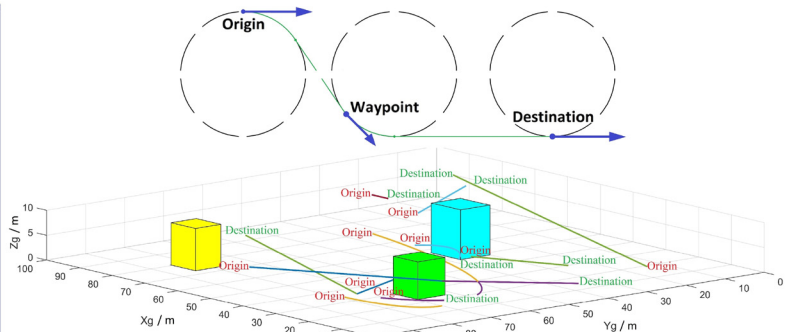
- Predict each trajectory independently on the most efficient route from origin to destination;
- Use the safety distance value to avoid proximate obstacles such as buildings;
- Take UAV state constraints and operational limitations into consideration;
- Take environment conditions and other global constraints into consideration.

**Table 3**  
Previous methods supporting strategic TP.

Category	Year	Method name	Method innovation
Graph search-based planning	1959	Dijkstra	The first path search method
	1968	A-star ( $A^*$ ) [35]	The first heuristic function with a cost term
	1994	D-star	Adapt to unknown surrounding environments
Local path planning	1986	Artificial potential field	Consider movements as a result of forces
	1998	Dynamic window approach	Score paths through an evaluation function
Sampling planning	1996	Probabilistic roadmap	Solve the local minimum problem [34]
	1996	Rapid-extended random tree	



(a) The taxiing path generated by the RRT method

(b) The flight trajectories generated by the  $A^*$  approach and Dubins curves**Fig. 6.** The taxiing path and flight trajectories.

Based on these principles, this section needs to select the most suitable method for strategic TP. According to their development trends, previous methods [34,35] are listed in Table 3.

In the problem with global constraints, the sampling planning method is more efficient than other methods. The Rapid-extended Random Tree (RRT) algorithm is the representative of this method, and it is selected for strategic TP in taxiing phases because of the following reasons.

(1) The RRT method is suitable for taxiing phases instead of flight phases, because it generates new tree branches connecting the nodes (on the existing tree), where the turning radius is close to zero. When UAVs taxi on the ground, their wheels play a key role in the advancement of taxiing performance. Conventional cylindrical wheels cannot complete lateral movements, and spherical tires are the new-generation tires due to their essential omnidirectional properties. The spherical wheels use magnetic levitation to suspend the fuselage over the wheels to realize a 360-degree turning angle, which conforms to the turning angle of the branches generated by the RRT method.

(2) The RRT method has a higher efficiency than the other methods, because the branches of the tree of the RRT method can be pre-computed to save computation costs [34].

(3) The new TP model will be compared with previous models [36] which use the RRT method for TP. To emphasize the development of the other parts (in addition to the RRT method) in the TP model, the new model also uses the RRT method to output UAV trajectories.

The  $A^*$  approach is selected for strategic TP in flight because of the following reasons.

(1) The  $A^*$  approach is suitable for flying UAVs to plan feasible trajectories considering constraints in cluttered environments, where the detected boundary is continuously added.

(2) The  $A^*$  approach increases the efficiency of the search by using the least heuristic cost, which is the remaining Euclidean distance between the node and goal.

(3) The new TP model will be compared with previous models that use the  $A^*$  approach for TP [36]; thus, it also uses the  $A^*$  approach to output UAV trajectories to emphasize the development of the other parts (in addition to the  $A^*$  approach) in the TP model.

In Fig. 6(a), the turning radius of the taxiing path generated by the RRT method can be zero. The flight trajectories generated by the  $A^*$  approach have steering angle and turning radius constraints; thus, Dubins curves are used to obtain smooth and flyable trajectories in Fig. 6(b).

Usually, the practical problem needs not only feasible long-term trajectories but also realistic short-term trajectory segments. The latter can be obtained by tactical TP models as follows.

#### 4.2. Tactical Trajectory Prediction model development

Tactical TP is used for short-term predictions which might be affected by small errors; thus, it requires as much operational information as possible for immediate response. The new tactical TP model is derived from aerodynamic formulas and Newton's second law of motion and written as 6-dimension-of-freedom VDMs. To mitigate TP errors, this model incorporates the quasi-steady method to calculate the aerodynamic forces based on the real-time UAV configuration.

When a UAV moves on the ground in a taxiing phase, the ground reaction forces are all applied on its wheel-ground interfaces. A new generic VDM is required to make UAVs mechanically and systematically simpler. The VDM contains certain parts: a fuselage, landing struts, and wheels. Before the establishment of the VDM, several coordinate systems are defined as follows.

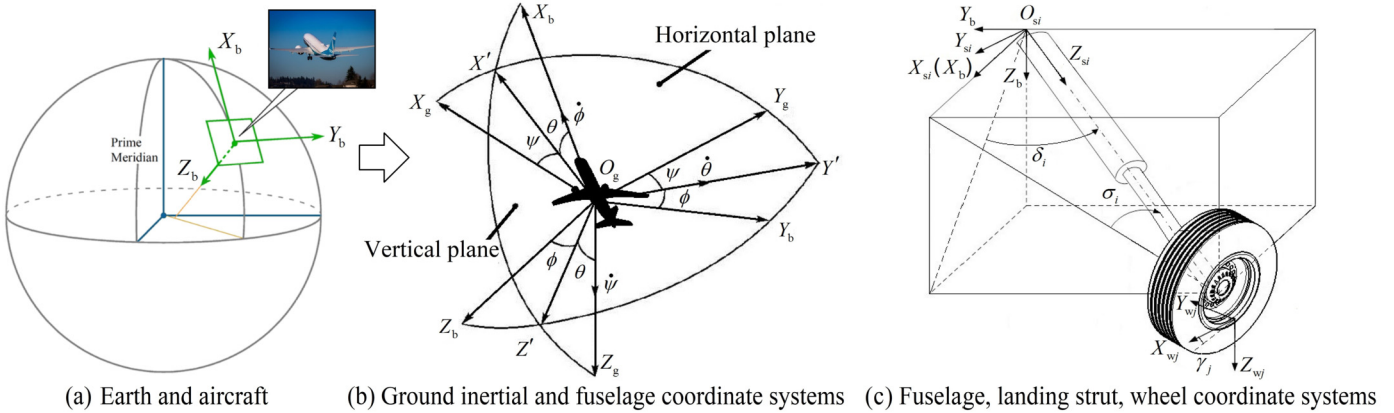


Fig. 7. The relationships of coordinate systems.

- Ground Inertial Coordinate System (GICS) (denoted by  $O_g - X_g Y_g Z_g$ ) is fixed to the ground.
- Fuselage Coordinate System (FCS) (denoted by  $O_b - X_b Y_b Z_b$ ) is fixed to the centre-of-gravity of the UAV.
- Representation with  $i$ th Landing Strut Coordinate System (LSCS)  $O_{si} - X_{si} Y_{si} Z_{si}$  ( $i = 1, 2, \dots, n$ ): The coordinate origin  $O_{si}$  is the connection point between the  $i$ th landing strut and fuselage.
- Representation with  $j$ th Wheel Coordinate System (WCS)  $O_{wj} - X_{wj} Y_{wj} Z_{wj}$  ( $j = 1, 2, \dots, m$ ): The coordinate origin  $O_{wj}$  is fixed to the centre of the  $j$ th wheel-ground interface.

The coordinate transformation matrix from the FCS to the GICS (denoted by  $\mathbf{M}_{gb}$ ) is described via Euler angles (i.e., pitch, yaw, and roll angles, denoted by  $\theta, \psi, \phi$ ) and denoted as:

$$\mathbf{M}_{gb} = \mathbf{M}_x(\phi) \mathbf{M}_y(\theta) \mathbf{M}_z(\psi) = \begin{bmatrix} \cos \theta \cos \psi & \sin \phi \sin \theta \cos \psi - \cos \phi \sin \psi & \cos \phi \sin \theta \cos \psi + \sin \phi \sin \psi \\ \cos \theta \sin \psi & \sin \phi \sin \theta \sin \psi + \cos \phi \cos \psi & \cos \phi \sin \theta \sin \psi - \sin \phi \cos \psi \\ -\sin \theta & \sin \phi \cos \theta & \cos \phi \cos \theta \end{bmatrix} \quad (3)$$

The transformation matrix from the FCS to the  $i$ th LSCS (denoted by  $\mathbf{M}_{sib}$ ) is denoted as:

$$\mathbf{M}(\delta_i) \mathbf{M}(\sigma_i) = \begin{bmatrix} \cos \sigma_i & 0 & -\sin \sigma_i \\ -\sin \sigma_i \sin \delta_i & \cos \delta_i & -\cos \sigma_i \sin \delta_i \\ \sin \sigma_i \cos \delta_i & \sin \delta_i & \cos \sigma_i \cos \delta_i \end{bmatrix} \quad (4)$$

The transformation matrix from the GICS to the  $j$ th WCS (denoted by  $\mathbf{M}_{wjq}$ ) is denoted as:

$$\mathbf{M}_{wjq} = \begin{bmatrix} \cos \theta \cos (\psi + \gamma_j) & \cos \theta \sin (\psi + \gamma_j) & -\sin \theta \\ -\sin (\psi + \gamma_j) & \cos (\psi + \gamma_j) & 0 \\ \sin \theta \cos (\psi + \gamma_j) & \sin \theta \sin (\psi + \gamma_j) & \cos \theta \end{bmatrix} \quad (5)$$

The relationships of different coordinate systems are shown in Fig. 7.

The dynamic movement of each UAV is decoupled to dynamic translation and rotation equations. The dynamic translation equation of the UAV fuselage in the GICS is denoted as:

$$m_b \begin{bmatrix} \ddot{x}_b \\ \ddot{y}_b \\ \ddot{z}_b \end{bmatrix} = \mathbf{M}_{gb} \left\{ -\sum_{i=1}^n \mathbf{M}_{sib}^{-1} \begin{bmatrix} F_{xi} \\ F_{yi} \\ F_{zi} \end{bmatrix} + \begin{bmatrix} -D \\ C \\ H \end{bmatrix} \right\} + \begin{bmatrix} 0 \\ 0 \\ W_b \end{bmatrix} \quad (6)$$

The dynamic rotation equation of the UAV fuselage in the FCS is denoted as:

$$\mathbf{I}_b \begin{bmatrix} \dot{\omega}_x \\ \dot{\omega}_y \\ \dot{\omega}_z \end{bmatrix} = - \begin{bmatrix} 0 & -\omega_z & \omega_y \\ \omega_z & 0 & -\omega_x \\ -\omega_y & \omega_x & 0 \end{bmatrix} \mathbf{I}_b \begin{bmatrix} \omega_x \\ \omega_y \\ \omega_z \end{bmatrix} + \sum_{i=1}^n \mathbf{M}_{sib}^{-1} \begin{bmatrix} T_{xi} \\ T_{yi} \\ T_{zi} \end{bmatrix} + \sum_{i=1}^n \begin{bmatrix} 0 & -z_{si} & y_{si} \\ z_{si} & 0 & -x_{si} \\ -y_{si} & x_{si} & 0 \end{bmatrix} \mathbf{M}_{sib}^{-1} \begin{bmatrix} F_{xi} \\ F_{yi} \\ F_{zi} \end{bmatrix} \\ + \begin{bmatrix} 0 & -z_c & y_h \\ z_d & 0 & -x_h \\ -y_d & x_c & 0 \end{bmatrix} \begin{bmatrix} -D \\ C \\ H \end{bmatrix} \quad (7)$$

where  $m_b$  and  $\mathbf{I}_b$  are the mass and moment of inertia of the UAV fuselage;  $x_{si}, y_{si}, z_{si}$  are the distances from the UAV centre-of-gravity to the junction point of the  $i$ th landing strut along  $O_b - X_b, O_b - Y_b, O_b - Z_b$  directions;  $[F_{xi}, F_{yi}, F_{zi}]^T$  and  $[T_{xi}, T_{yi}, T_{zi}]^T$  are the force and torque vectors;  $\omega_x, \omega_y, \omega_z$  are the UAV angular speeds along  $O_b - X_b, O_b - Y_b, O_b - Z_b$  directions;  $[\ddot{x}_b, \ddot{y}_b, \ddot{z}_b]^T$  is the acceleration vector of the UAV fuselage;  $[0, 0, W_b]^T$  is the gravitational force vector of the UAV fuselage;  $[-D, C, H]^T$  is the wind force vector;  $y_d$  and  $z_d$  are the distances from UAV centre to line of force  $D$  along  $O_b - Y_b$  and  $O_b - Z_b$ ;  $x_c$  and  $z_c$  are the distances from UAV centre to line of force  $C$  along  $O_b - X_b$  and  $O_b - Z_b$ ;  $x_h$  and  $y_h$  are the distances from UAV centre to line of force  $H$  along  $O_b - X_b$  and  $O_b - Y_b$ .

The transformation from the derivative of the UAV attitude in the GICS (denoted by  $\dot{\psi}, \dot{\theta}, \dot{\phi}$ ) to the UAV angular velocity in the FCS (denoted by  $\omega_x, \omega_y, \omega_z$ ) is denoted as:

$$\begin{bmatrix} \omega_x \\ \omega_y \\ \omega_z \end{bmatrix} = \begin{bmatrix} -\sin\theta & 0 & 1 \\ \cos\theta \sin\phi & \cos\phi & 0 \\ \cos\theta \cos\phi & -\sin\phi & 0 \end{bmatrix} \begin{bmatrix} \dot{\psi} \\ \dot{\theta} \\ \dot{\phi} \end{bmatrix} \quad (8)$$

The dynamic translation equation of the  $i$ th landing strut is denoted as:

$$m_i \begin{bmatrix} \ddot{x}_{si} \\ \ddot{y}_{si} \\ \ddot{z}_{si} \end{bmatrix} = \mathbf{M}_{gb} \mathbf{M}_{sib}^{-1} \begin{bmatrix} F_{xi} \\ F_{yi} \\ F_{zi} \end{bmatrix} + \sum_{j=2i-1}^{2i} \mathbf{M}_{wjj}^{-1} \begin{bmatrix} F_{fj} \\ F_{cj} \\ F_{nj} \end{bmatrix} + \begin{bmatrix} 0 \\ 0 \\ W_i \end{bmatrix} \quad (9)$$

The dynamic rotation equation of the  $j$ th wheel in the  $j$ th WCS is denoted as:

$$\mathbf{I}_{wj} \begin{bmatrix} \ddot{\varphi}_j \\ \ddot{\gamma}_j \end{bmatrix} = \begin{bmatrix} T_j - (r_j - \varepsilon_j) F_{fj} \\ 0.85\zeta(\alpha_j) \sqrt{(2\varepsilon_j r_j - \varepsilon_j^2)} F_{cj} \end{bmatrix} - \begin{bmatrix} T_{xwj} \\ T_{ywj} \end{bmatrix} \quad (10)$$

where  $m_i$  and  $W_i$  are the mass and gravitational force of the  $i$ th landing strut;  $[\ddot{x}_{si}, \ddot{y}_{si}, \ddot{z}_{si}]^T$  is the acceleration vector of the  $i$ th landing strut;  $\mathbf{I}_{wj}$  is the moment of inertia of the  $j$ th wheel;  $[\ddot{\varphi}_j, \ddot{\gamma}_j]^T$  is the angular acceleration vector of the  $j$ th wheel;  $T_j$  is the driving torque of the  $j$ th wheel;  $T_{xwj}$  and  $T_{ywj}$  are the rolling and aligning resistance moments of the  $j$ th wheel;  $r_j$  and  $\varepsilon_j$  are the radius and vertical deflection of the  $j$ th wheel;  $\alpha_j$  and  $\zeta(\alpha_j)$  are the lateral force coefficient and aligning torque coefficient of the  $j$ th wheel;  $F_{nj}$  is the normal force;  $F_{fj}$  and  $F_{cj}$  are the rolling friction force along  $O_{wj} - X_{wj}$  and lateral friction force along  $O_{wj} - Y_{wj}$ .

Equations (6) and (9) are integrated into the UAV dynamic translation equation in the GICS.

$$\left( m_b + \sum_{i=1}^n m_i \right) \begin{bmatrix} \ddot{x} \\ \ddot{y} \\ \ddot{z} \end{bmatrix} = \sum_{j=1}^m \mathbf{M}_{wjj}^{-1} \begin{bmatrix} F_{fj} \\ F_{cj} \\ F_{nj} \end{bmatrix} + \mathbf{M}_{gb} \begin{bmatrix} -D \\ C \\ H \end{bmatrix} + \begin{bmatrix} 0 \\ 0 \\ W_b + \sum_{i=1}^3 W_i \end{bmatrix} \quad (11)$$

Equation (11) is transformed into the UAV dynamic translation equation in the FCS.

$$\left( m_b + \sum_{i=1}^n m_i \right) \begin{bmatrix} \ddot{x}'' \\ \ddot{y}'' \\ \ddot{z}'' \end{bmatrix} = \sum_j \mathbf{M}_{gb}^{-1} \mathbf{M}_{wjj}^{-1} \begin{bmatrix} F_{fj} \\ F_{cj} \\ 0 \end{bmatrix} + \sum_j \mathbf{M}_{gb}^{-1} \mathbf{M}_{wjj}^{-1} \begin{bmatrix} 0 \\ 0 \\ F_{nj} \end{bmatrix} + \begin{bmatrix} -D \\ C \\ H \end{bmatrix} + \left( W_b + \sum_{i=1}^n W_i \right) \begin{bmatrix} -\sin\theta \\ \sin\phi \cos\theta \\ \cos\phi \cos\theta \end{bmatrix} \quad (12)$$

where  $[\ddot{x}, \ddot{y}, \ddot{z}]^T$  and  $[\ddot{x}'', \ddot{y}'', \ddot{z}'']^T$  are the acceleration vectors of the whole UAV in the GICS and FCS, which are accumulated to obtain the UAV trajectory.  $[\ddot{x}'', \ddot{y}'', \ddot{z}'']^T$  is denoted as:

$$\begin{bmatrix} \ddot{x}'' \\ \ddot{y}'' \\ \ddot{z}'' \end{bmatrix} = \begin{bmatrix} \ddot{\varphi}_j (r_j - \varepsilon_j) \\ \ddot{x} (\sin\phi \sin\theta \cos\psi - \cos\phi \sin\psi) + \ddot{z} \sin\phi \cos\theta + \ddot{y} (\sin\phi \sin\theta \sin\psi + \cos\phi \cos\psi) \\ \ddot{x} (\cos\theta \cos\psi) + \ddot{y} (\cos\theta \sin\psi) - \ddot{z} \sin\theta \end{bmatrix} \quad (13)$$

When a UAV flies in the air, the aerodynamic forces applied on its flight components change its position. The dynamic translation equation of the whole UAV in the GICS is denoted as:

$$\left( m_b + \sum_{i=1}^n m_i \right) \begin{bmatrix} \ddot{x}_b \\ \ddot{y}_b \\ \ddot{z}_b \end{bmatrix} = \mathbf{M}_{gb} \begin{bmatrix} T \\ R \\ -L \end{bmatrix} + \mathbf{M}_{gb} \begin{bmatrix} -D \\ C \\ H \end{bmatrix} + \begin{bmatrix} 0 \\ 0 \\ W_b \end{bmatrix} \quad (14)$$

The dynamic rotation equation of the whole UAV in the FCS is denoted as:

$$\begin{aligned} \left( \mathbf{I}_b + \sum_{j=1}^m \mathbf{I}_{wj} \right) \begin{bmatrix} \dot{\omega}_x \\ \dot{\omega}_y \\ \dot{\omega}_z \end{bmatrix} = & - \begin{bmatrix} 0 & -\omega_z & \omega_y \\ \omega_z & 0 & -\omega_x \\ -\omega_y & \omega_x & 0 \end{bmatrix} \left( \mathbf{I}_b + \sum_{j=1}^m \mathbf{I}_{wj} \right) \begin{bmatrix} \omega_x \\ \omega_y \\ \omega_z \end{bmatrix} + \begin{bmatrix} 0 & -z_r & y_l \\ z_t & 0 & -x_l \\ -y_t & x_r & 0 \end{bmatrix} \begin{bmatrix} T \\ R \\ -L \end{bmatrix} \\ & + \begin{bmatrix} 0 & -z_c & y_h \\ z_d & 0 & -x_h \\ -y_d & x_c & 0 \end{bmatrix} \begin{bmatrix} -D \\ C \\ H \end{bmatrix} \end{aligned} \quad (15)$$

where  $[T, R, -L]^T$  is aerodynamic forces;  $y_t$  and  $z_t$  are distances from UAV centre to line of force  $T$  along  $O_b - Y_b$  and  $O_b - Z_b$ ;  $x_r$  and  $z_r$  are distances from UAV centre to line of force  $R$  along  $O_b - X_b$  and  $O_b - Z_b$ ;  $x_l$  and  $y_l$  are distances from UAV centre to line of force  $L$  along  $O_b - X_b$  and  $O_b - Y_b$ .

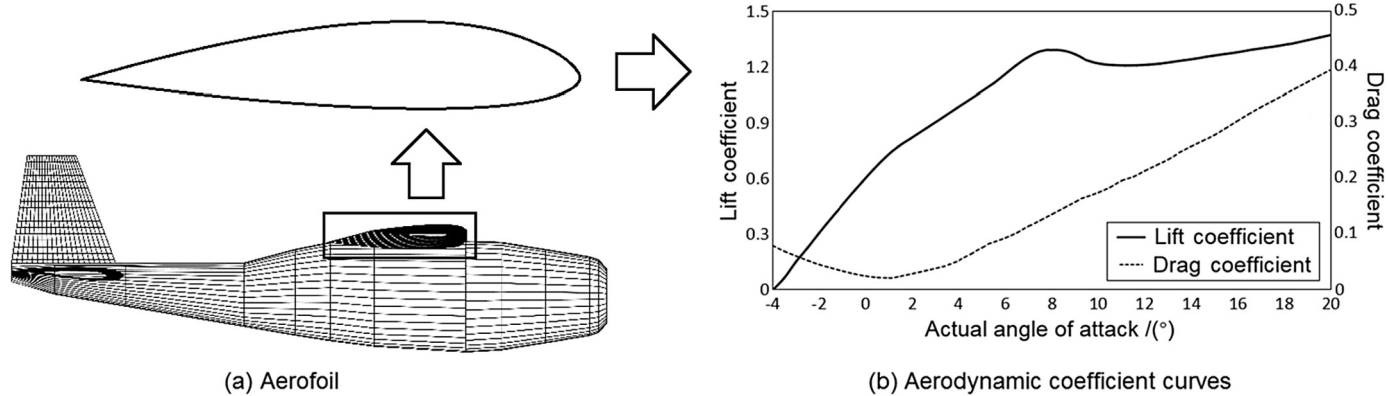


Fig. 8. Aerodynamic lift and drag coefficients.

**Table 4**  
UAV applications and environments.

Environment	UAV application	Low dynamic	Highly dynamic
	Static application		
Military space	<b>No static military use</b>	Military surveillance	Dynamic military uses
Civil airspace	Media platform ( <b>future</b> )	Inspection	Mapping and surveying
Suburban area	Commercial uses	Agricultural uses	Logistics
Urban airspace	Urban industrial uses	Emergency response	Humanitarian delivery
Urban ground	Safety uses	Urban passenger transport ( <b>future</b> )	

#### 4.3. Vehicle performance modelling development

A quasi-steady method is applied to calculate the aerodynamic force vector  $[T, R, -L]^T$ :

$$\begin{bmatrix} T \\ R \\ -L \end{bmatrix} = \left\{ \begin{array}{l} \sum_{k=1}^K \int_0^{P_k} \frac{1}{P} \int_0^{b_k} \frac{1}{2} \rho |\mathbf{v}_\infty + \mathbf{v}_f|^2 [C_l(\alpha) \sin(\alpha) - C_d(\alpha) \sin(\alpha)] c(l) dl dt \\ \sum_{k=1}^K \int_0^{P_k} \frac{1}{P} \int_0^{b_k} \frac{1}{2} \rho |\mathbf{v}_\infty + \mathbf{v}_f|^2 [C_l(\alpha) \cos(\alpha) + C_d(\alpha) \sin(\alpha)] \sin(\beta) c(l) dl dt \\ - \sum_{k=1}^K \int_0^{P_k} \frac{1}{P} \int_0^{b_k} \frac{1}{2} \rho |\mathbf{v}_\infty + \mathbf{v}_f|^2 [C_l(\alpha) \cos(\alpha) + C_d(\alpha) \sin(\alpha)] \cos(\beta) c(l) dl dt \end{array} \right\} \quad (16)$$

where  $P_k$  is the period of a rotational cycle of the  $k$ th rotor or propeller (s);  $b_k$  is the total length of the  $k$ th rotor or propeller (m) among the set of flight components  $K$ ;  $\rho$  is atmospheric density ( $\text{kg}/\text{m}^3$ );  $\mathbf{v}_\infty$  is the level flight velocity (m/s);  $\mathbf{v}_f$  is the linear velocity of a studied aerofoil of the rotor or propeller (m/s);  $l$  is the distance from the studied aerofoil to the root of the rotor or propeller (m);  $c(l)$  is the chord of the studied aerofoil (m), which varies with the distance  $l$  (m);  $\beta$  is the camber angle (rad);  $\alpha$  is the angle of attack of the studied aerofoil (rad). When the Reynolds number is set to be 100000, the lift coefficient (denoted by  $C_l(\alpha)$ ) and drag coefficient (denoted by  $C_d(\alpha)$ ) of the aerofoil against the angle of attack (denoted by  $\alpha$ ) are shown in Fig. 8.

#### 5. Validation and demonstration of Trajectory Prediction models

For the demonstration of the new TP model in different UAV applications, three credible case studies are specified and implemented, and TP accuracy is quantified. In different applications, the TP model needs to fulfil various levels of accuracy requirements. It is hard to build TP models for all current and future UAV applications to fulfil their specific accuracy requirements; thus, the most stringent applications are considered in the specification of case studies. If the TP model supports the most stringent applications, it will also be able to support the other applications.

Current UAV applications [25] are categorised into military uses, agricultural uses, industrial uses, safety uses, commercial uses, emergency response, inspection, mapping, surveying, logistics, and humanitarian delivery. Future UAV applications are categorised into media platforms and urban passenger transport. According to their operational environments and the levels of dynamics, all the UAV applications are consolidated into an exhaustive list in Table 4.

The accuracy requirement represents the upper limit of position errors, and it is related to the population and property densities in the UAV operational environment. Urban spaces have higher population and property densities than suburban spaces; thus, they require more accurate UAV operations to avoid collisions with people or properties. Additionally, the accuracy requirement is affected by the speed of the wind, which is an important uncertainty factor and error source. The wind speeds in urban spaces are normally lower than civil airspaces; thus, the UAV operations within the geographical limits of urban spaces are able to fulfil higher-level accuracy requirements.



**Fig. 9.** The studied HTOL UAV.

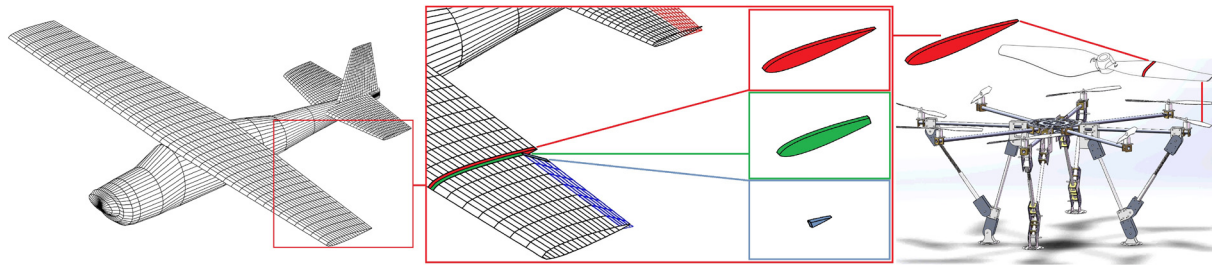


**Fig. 10.** The changing wing and tail configurations.

Logistics and humanitarian delivery and urban passenger transport applications have the most stringent accuracy requirements because they require highly dynamic UAV operations in suburban or urban spaces, which are filled with not only people and properties on the ground but also obstructions higher than UAVs. In such applications, UAV TP aims to fulfil the highest-level accuracy requirement to avoid collisions; thus, they are determined as the most stringent applications.

### 5.1. Case study for the most stringent suburban application: logistics

Logistics needs to be economical and punctual; thus, HTOL UAVs are the best choice due to their advantages: low-cost design, high power efficiency, and high speed.

The wingspan of the studied HTOL UAV is 3.6 m, and its full length is 2.05 m. The wing area of the UAV is 0.127 m<sup>2</sup>, and its take-off weight is 20 kg. The flight speed of the UAV is set to be 35 m/s, and it autonomously flies in a 10 km × 10 km × 1 km space. Visual navigation and Real Time Kinematic (RTK) dual link systems are used to measure UAV states with decimetre-level accuracy. See Fig. 9.

The wireframe model the UAV is built, and the quasi-steady method is applied to calculate the instantaneous aerodynamic performance of the changing wing and tail configurations. See Fig. 10.

The TP model outputs the predicted trajectory, which is compared with the trajectory obtained from the flight test. For the quantitative analysis of TP accuracy, this paper calculates the deviations between the actual and predicted trajectories to output TP errors as shown in Fig. 11. The accuracy requirement of the new TP model is specified at the 95th percentile of the position errors, i.e., the probability that a position error is within the accuracy requirement should be at least 95%.

The horizontal and vertical accuracy requirements are 130.900 m and 65.904 m, and the total accuracy requirement of the new TP model is 146.555 m. To compare the new model with previous models in terms of TP accuracy, Equation (2) is used to calculate the total error budget for previous models, which is 395.273 m. The new model has higher TP accuracy than previous models.

The attitudes and attitude errors of the TP model are shown in Fig. 12.

The attitudes outputted by the model are in conformance to the flight test results. The roll, pitch, and yaw accuracy requirements specified at the 95th percentiles are 5.803°, 3.014°, and 7.118°; thus, the total attitude accuracy requirement specified at the 95th percentile is 8.316°.

### 5.2. Case study for the most stringent current application: humanitarian delivery

Humanitarian delivery requires UAVs to replace surface vehicles if the roads are damaged in disasters. The post-disaster humanitarian delivery needs UAV trajectory information; thus, it calls for the capability of UAV TP. This application has the most stringent requirement on accuracy, because the essential items such as medicine need to be delivered to recipients accurately and punctually.

For the humanitarian delivery, hybrid UAVs are the best choice due to their advantages: high speed, dynamic operation, and no topography restriction for take-off and landing. Since the coronavirus pandemic began in 2020, there have also been many natural disasters; thus, pilots have coronavirus risk if they perform post-disaster humanitarian delivery manually. If the pilots stay at home to avoid coronavirus, the essential items can only be delivered by UAVs. This case study considers the UAV operations in taxiing and flight phases for humanitarian delivery.

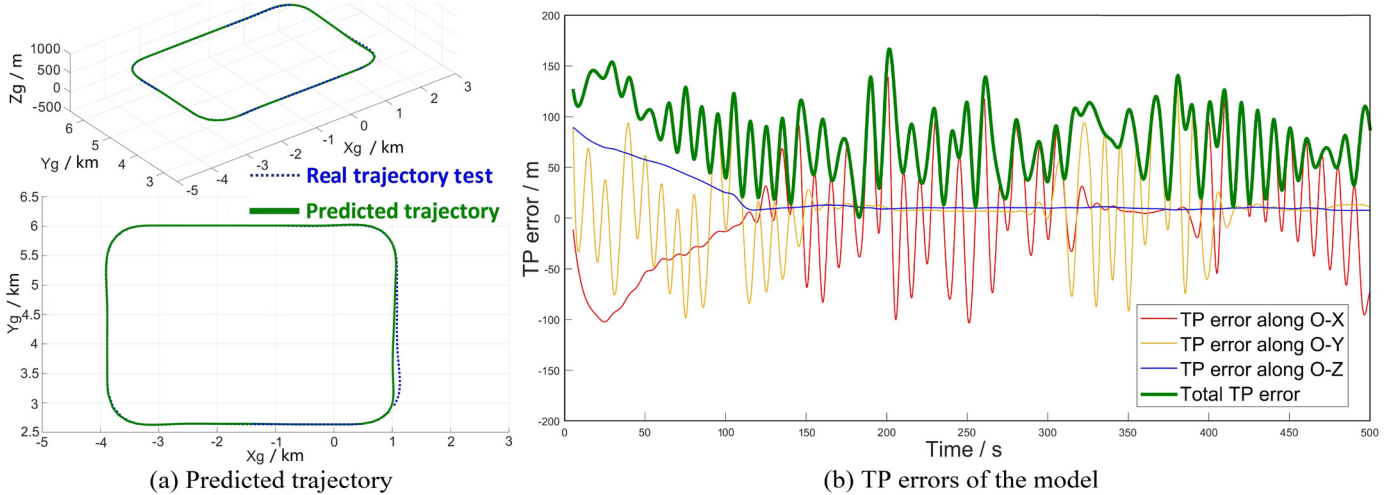


Fig. 11. The predicted trajectory and TP errors.

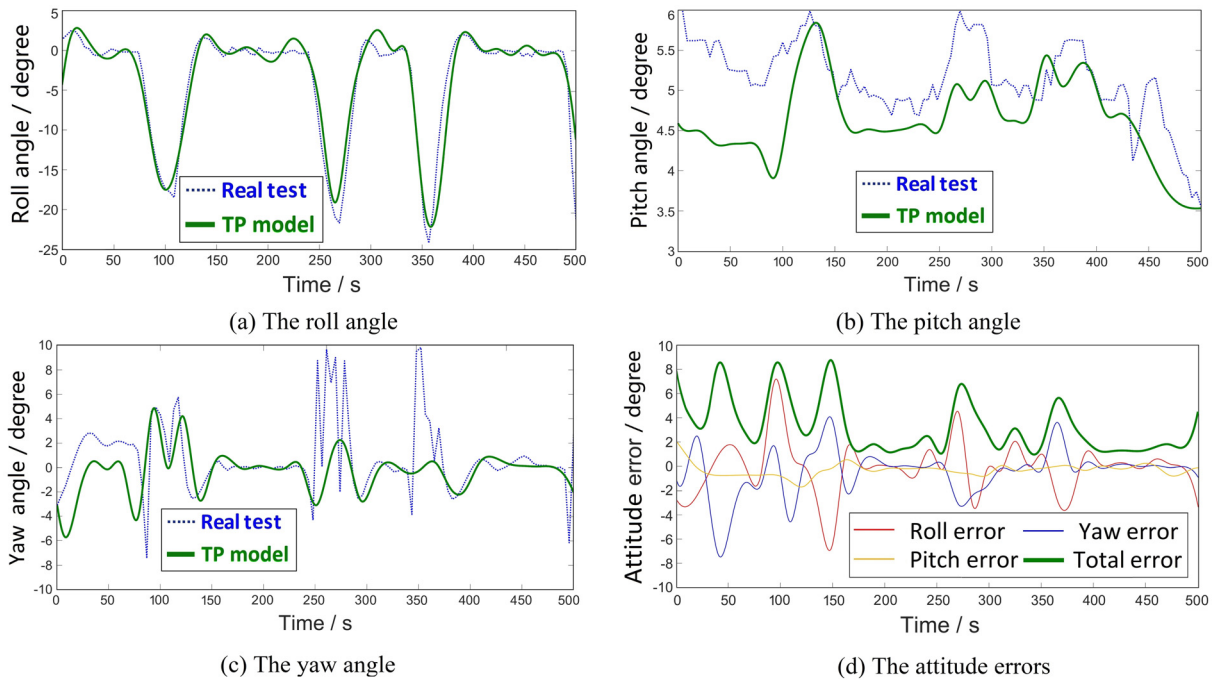


Fig. 12. The attitudes and attitude errors of the TP model.

In the taxiing phase, the UAV is driven by powered wheels and moves with a speed of 1 m/s (in the same way as autonomous vehicles). The 7.3-magnitude Chi-Chi earthquake in 1999 was one of the largest disasters recorded in East Asia over the past 30 years [36], with over 2000 casualties; thus, the post-disaster humanitarian delivery is studied in the environment of Chi-Chi. Before the TP process, the Chi-Chi map is transformed into a monochrome image as shown in Fig. 13.

For the new TP model, the environment can be changed. The new TP model is suitable for all environments, including different unknown scenarios (e.g., ash, ruins) because of following reasons.

(1) The post-disaster environments might be changed; however, according to the humanitarian delivery experience, the first work after each disaster is to detect the post-disaster environment as soon as possible. The post-disaster environment is detected in a short time, and then a fully realistic map is built by using mature environmental awareness techniques such as LiDAR. The representation of the environment can be generated by using the geographic data obtained from LiDAR surveys.

(2) If there are unknown things such as ash and ruins in the post-disaster environment, the TP model will autonomously consider that there is a blockage (at this location) in the route, and then the TP model will avoid UAVs approaching this area in simulations. This TP model ensures that all the locations of the unknown things such as ash and ruins need to be avoided by UAVs.

(3) Pilots and other people have risk in the post-disaster environments if they do post-disaster humanitarian delivery manually. The risk of the unknown environments (e.g., ash and ruins) needs to be reduced to zero, because pilots and other people are the most important. UAVs are increasingly used to do post-disaster humanitarian delivery autonomously without pilots or other people. If the essential items are delivered by autonomous pilotless UAVs, the pilots and other people will have no risk and the delivery price will be cheaper. For UAVs,

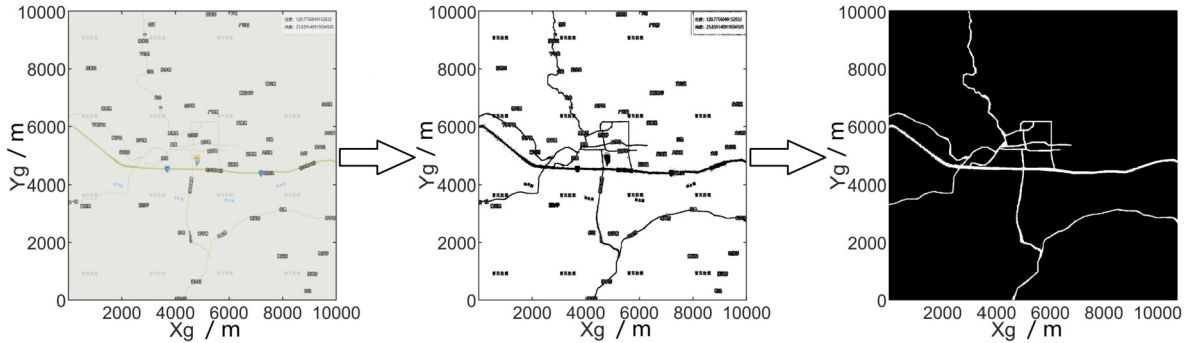


Fig. 13. The map of Chi-Chi.

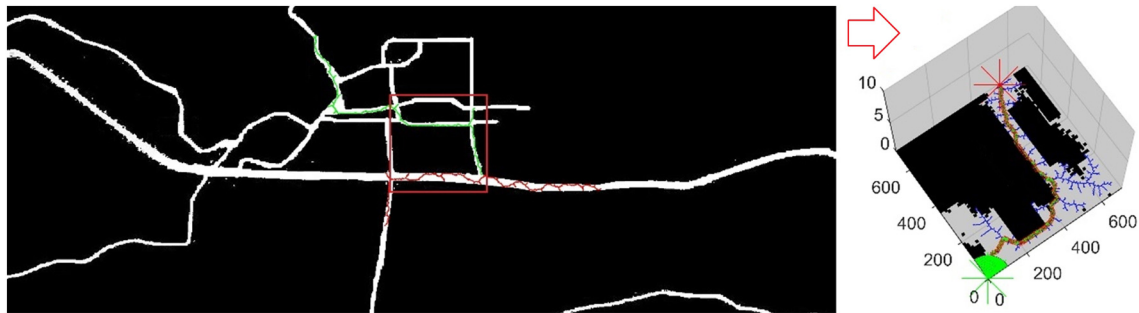


Fig. 14. The trajectory based on stochastically chosen origin and destination.

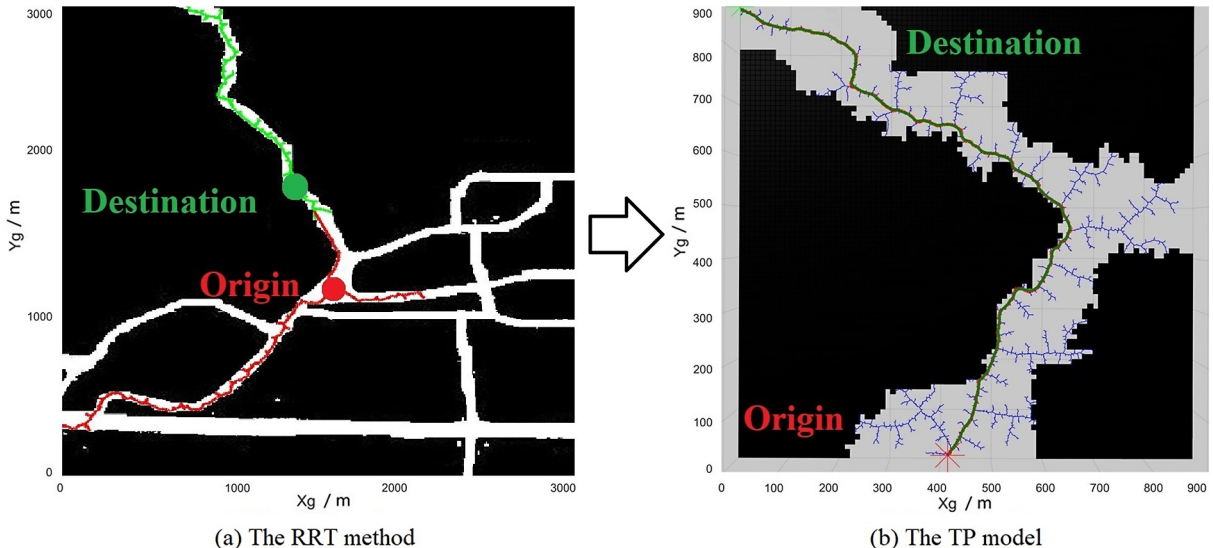


Fig. 15. The planned and predicted trajectories in the taxiing phase.

the risk of the unknown environments (e.g., ash and ruins) can be little higher than the environments for pilots and other people, because UAVs are not as important as the pilots or people in disaster areas (i.e., people are the most important).

The new TP model is suitable for all the situations and environments; thus, this case study can adopt any operational environments. For instance, this case study stochastically chooses the origin and destination, and then the TP model autonomously outputs the trajectory as shown in Fig. 14.

The previous model [36] is specified as the UAV operation after the Chi-Chi earthquake; thus, this case study selects the central Chi-Chi to be the operational environment to eliminate the influence of the environmental changes on the outputted trajectories and emphasize the development of the TP models. When the UAV taxis in a large area, its vertical speed and acceleration can be neglected; thus, the rolling and overturning moments exerted by the ground on the wheels can also be neglected. The RRT method outputs an open-loop path, and the TP model generates trajectory segments. See Fig. 15.

The TP errors of the new model are shown in Fig. 16. The accuracy requirement specified at the 95th percentile is 2.19 m. According to Equation (2), the trajectory modelling error is related to the taxiing distance during 8 s (i.e., 8 m), and the total error budget for previous models is 8.944 m; thus, the new model has higher TP accuracy than previous models.

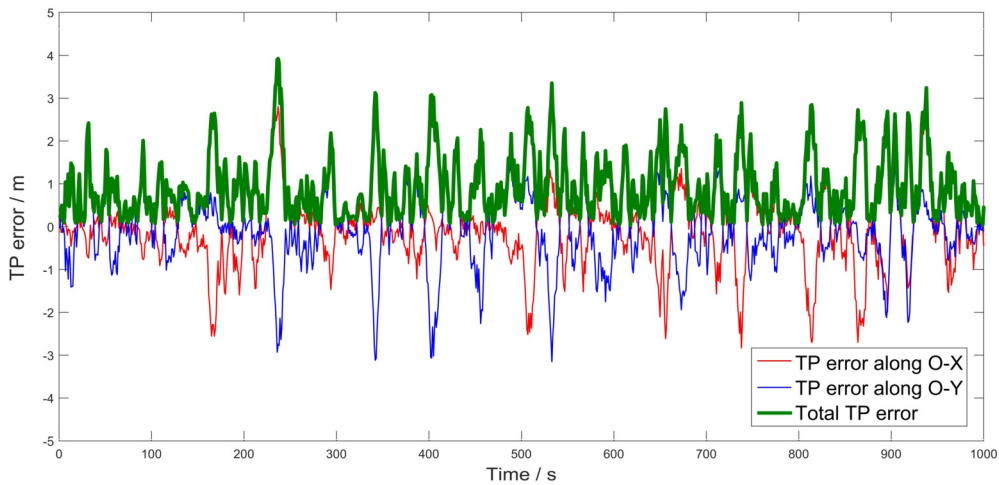


Fig. 16. TP errors in the taxiing phase.

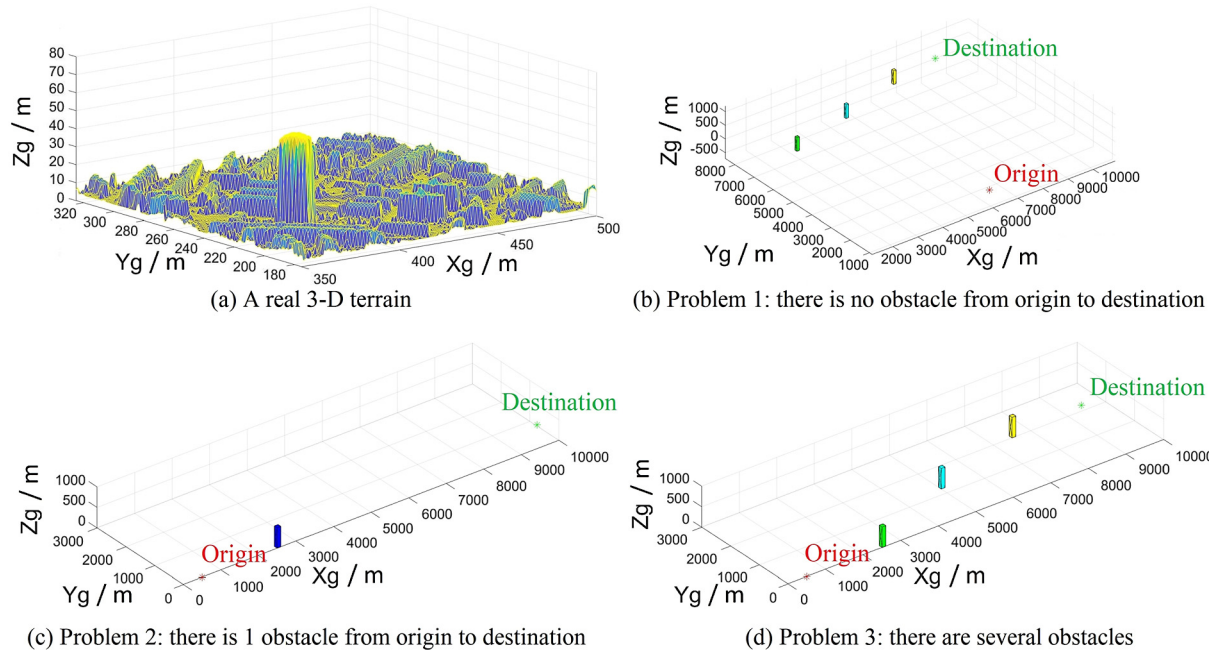


Fig. 17. The 3-D terrain and obstacle conditions.

In the flight phase, the UAV speed is set to be 50 m/s, which is same as previous research. Before the UAV flight, people first use LiDAR techniques to measure the heights of the terrain and surface objects such as buildings to generate the 3-Dimensional (3-D) terrain surface. The 3-D terrain surface includes complex obstacles; however, in order to ensure a higher level of safety, the boundary of each obstacle has been replaced by a larger cuboid. On the basis of a real 3-D terrain surface, this case study sets up three assumed problems considering different obstacles as shown in Fig. 17.

The studied UAV is the DeltaQuad hybrid UAV with four rotors, which is same as previous research [36]. The aerodynamic force is simplified to four force vectors which are generated by the four rotors. When the UAV flies in a 3-D space, it needs to avoid other objects such as buildings. See Fig. 18.

In Problem 1, the A\* approach outputs a relatively optimal path, and the new TP model is used to predict the UAV trajectory. The predicted trajectory of the new TP model is in conformance with previous models [36] in Fig. 19(a). The TP errors of the new model are shown in Fig. 19(b).

In Problem 2, the safety distance from the UAV to obstacles is set to be 500 m. Compared with previous models [36], the new TP model generates a shorter trajectory as shown in Fig. 20.

In Problem 3, the safety distance is set to be 1000 m because there are many obstacles. Compared with previous models [36], the new TP model generates a shorter trajectory in Fig. 21.

The distances from the obstacles to the outputted waypoints of the previous model are more than the safety distance, showing that the previous model fails to converge to a globally optimal solution. Compared with the previous model, the new TP model generates a more suitable trajectory.

In Problem 3, the TP errors of the new model are shown in Fig. 22.

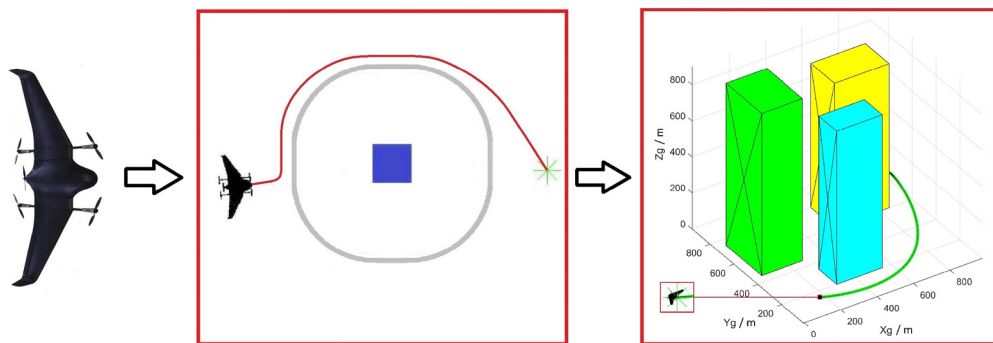


Fig. 18. The studied UAV for the flight phase of humanitarian delivery.

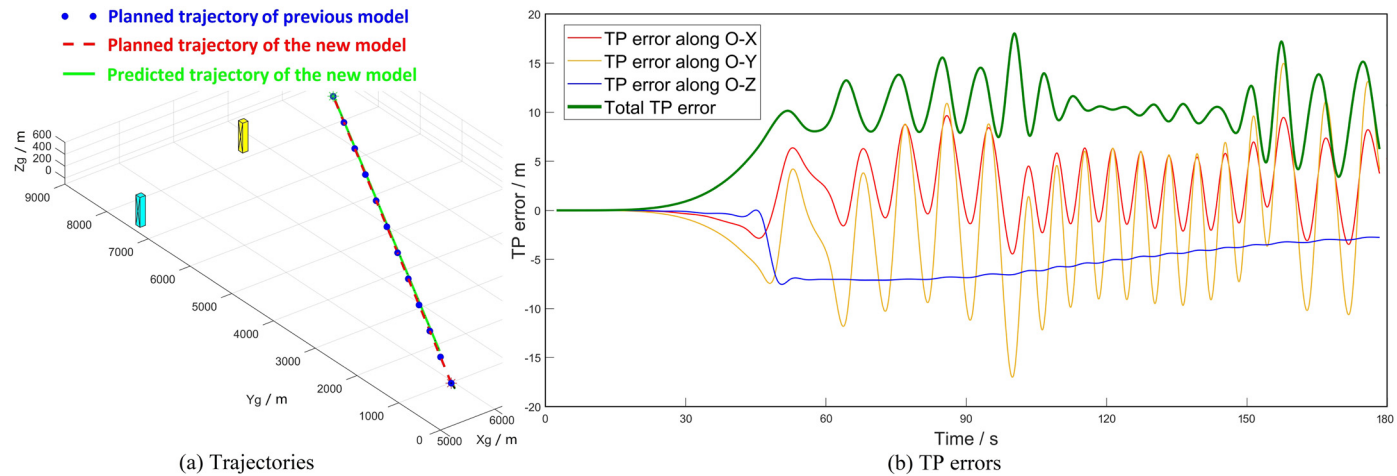


Fig. 19. Comparison of the new model with previous models in Problem 1.

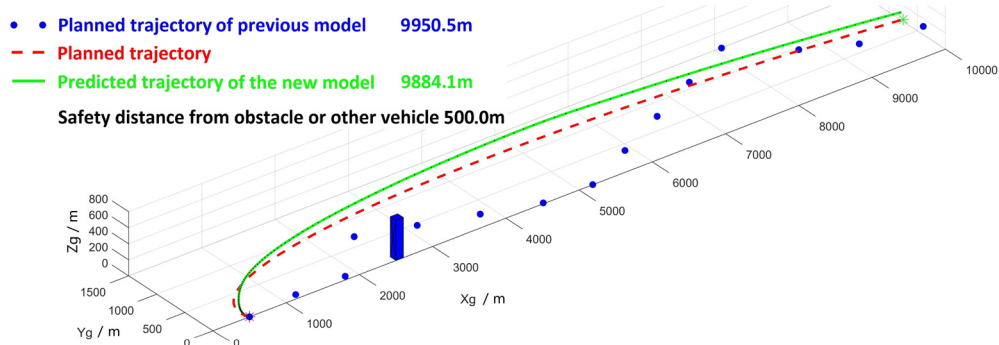


Fig. 20. Comparison of the new model with previous models in Problem 2.

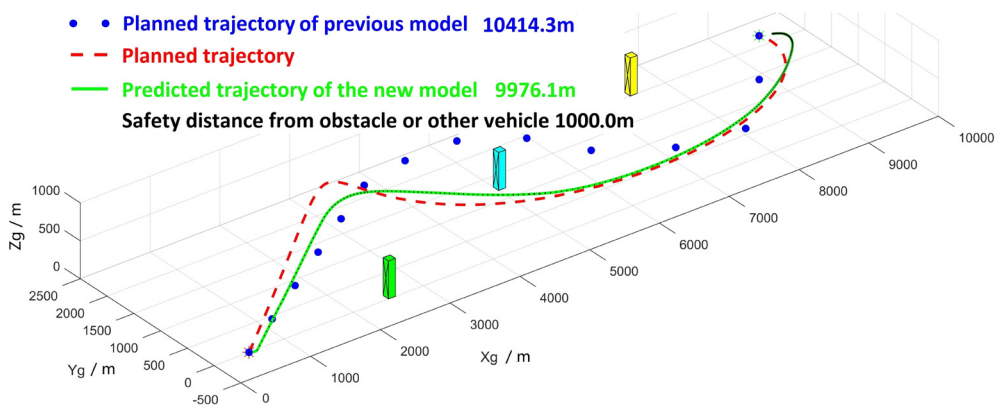


Fig. 21. Comparison of the new model with previous models in Problem 3.

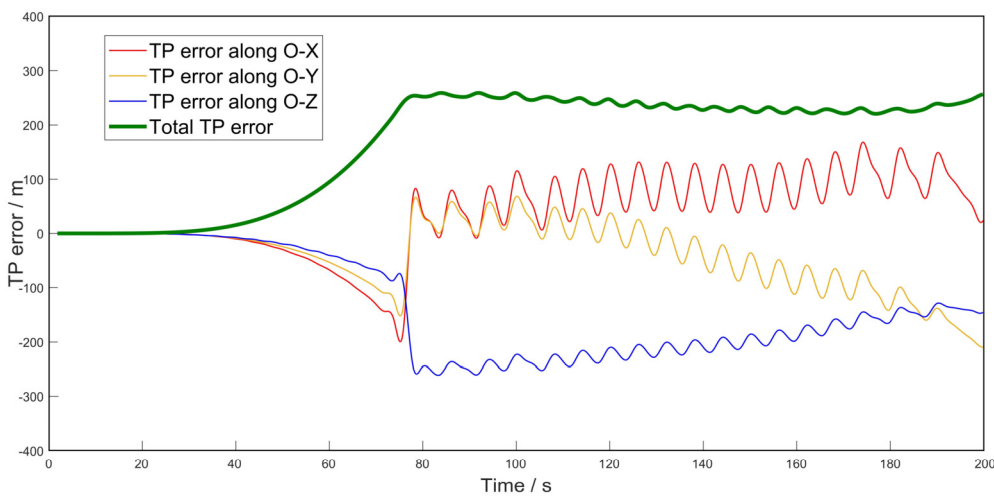


Fig. 22. TP errors in Problem 3.



Fig. 23. The full-scale and scaled passenger transport vehicles.

The horizontal and vertical accuracy requirements (specified at the 95th percentiles) of the new TP model are 224.2 m and 124.0 m; thus, its total accuracy requirement is 256.2 m. To compare the new model with previous models, Equation (2) is used to calculate the total error budget for previous models, which is 447 m; thus, the new model has higher TP accuracy than previous models.

### 5.3. Case study for the most stringent future application: urban passenger transport

Urban passenger transport is the most stringent future UAV application considering its society impact and safety criticality. Looking to tap into the potential of passenger transport, many start-ups have developed more than 100 roadable UAVs, most of which are VTOL UAVs with precise positioning capabilities. VTOL UAVs increase passenger safety and comfort due to their simple operations, altitude manoeuvrability and hovering capabilities.

Some passenger transport UAVs combine the advantages of surface and aerial vehicles. Some UAVs include both rotors and wheels. The taxiing phase of a UAV might have thousands of metres and last for hours; thus, the taxiing and flight phases are considered as two separate steps. According to their working principles, all of current passenger transport UAVs have two following similarities.

- In the taxiing phase, UAVs present great challenges owing to pedestrians and vehicles. UAVs are driven by powered wheels and move on the ground in the same way as autonomous vehicles.
- In the flight phase, UAVs are new objects in airspaces, and they need to avoid static and moving obstacles in the vicinity. In the flight process, UAVs are propelled by their rotors.

To bridge the automotive and aerospace domains, Airbus designed a modular ground and air passenger transport vehicle: Pop.Up [37], which includes a capsule coupling to an electric propelled module (i.e., either a ground or air module). The capsule is 2.6-metre long, 1.5-metre wide and 1.4-metre high, and it is carried by a 5 by 4.4 metre air module propelled by rotors. Based on user demands, the UAV automatically suggests the best transport solution: either flight or taxiing.

In the taxiing phase, a scaled prototype is required for ground movement tests, which are used to validate the performance of the new TP model. Airbus and Audi believe that passenger transport UAVs can be mass-produced and become the convenient means of transportation [37]; thus, they have jointly developed a 1/4 scale prototype and implemented its preliminary functions. See Fig. 23.

To validate the new TP model in the taxiing phase, this paper constructs the prototype to a (1/3)-dimensional scale and a (1/3)<sup>3</sup>-mass scale for taxiing tests. By using the technique of dynamic scaling, the scaled prototype has the desirable characteristics of being untethered, of having a convenient size for handling, and of having easily obtainable mass properties. The 1/3 scaled prototype is equipped with a



Fig. 24. The scaled prototype equipped with sensors.

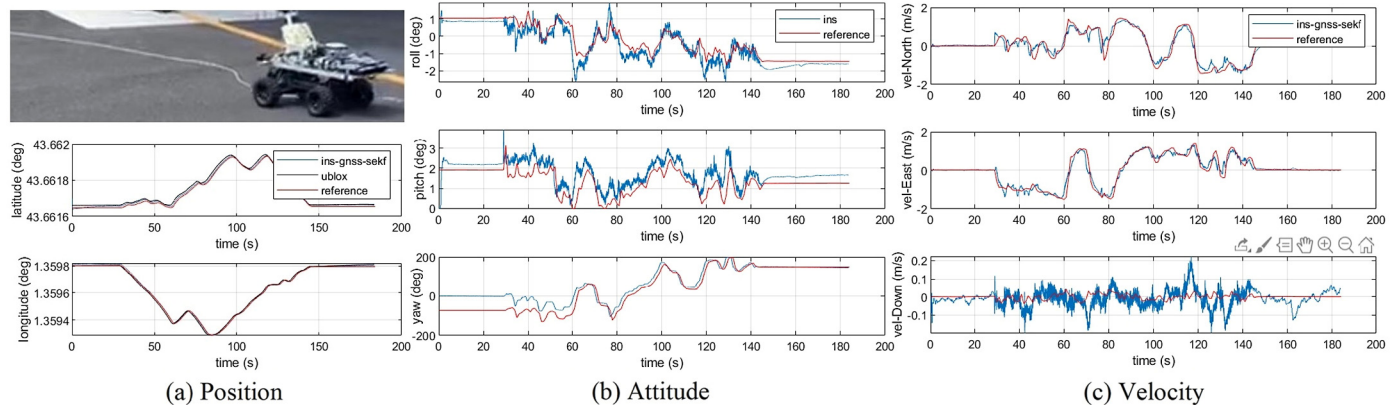


Fig. 25. The validation of measured states.

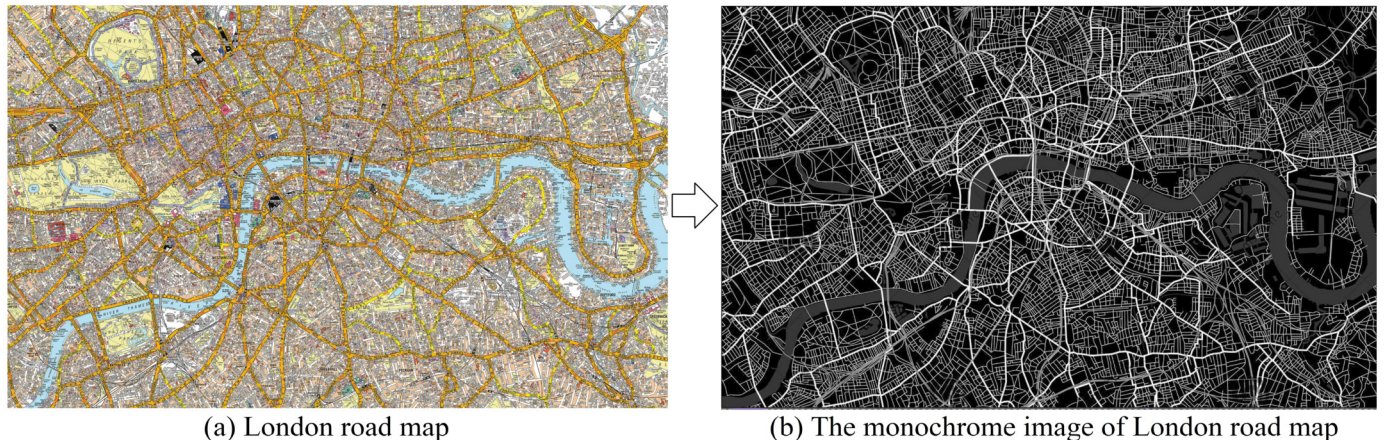


Fig. 26. The monochrome image of London road map.

high-grade integrated GNSS/INS/LiDAR/camera navigation system as shown in Fig. 24. The GNSS receivers and other sensors output the actual states of the scaled prototype, which are used together as a reference in the comparison with the predicted states.

Before the test, the accuracy of the integrated navigation system needs to be validated. The scaled prototype moves along a white referenced path that is pre-determined (i.e., the ground truth), and the integrated navigation system is used to measure its real-time states. The measured states are compared with their references, which have been post-processed with the backward and forward nonlinear smoothing to be considered as the actual states as shown in Fig. 25.

Fig. 25 shows that the integrated navigation system is able to fulfil decimetre-level accuracy requirements. The position accuracy is 0.2 m. The attitude accuracy is 0.3°. The speed accuracy is 0.05 m/s. These measured data can be considered as the references, which are compared with the results of the new model to analyse TP performance in terms of accuracy.

TP performance highly depends on contextual factors; thus, it is required to accurately map the real UAV operational environment. Generally, urban environments are more complicated than suburban environments, because they contain more obstacles. The overpopulated metropolitan cities such as London are the most complicated environments, and they contain many accessible geographic data; thus, they are the most suitable environments for the taxiing tests. In many downtown areas of London, the speed limit is 8.9 m/s; thus, the taxiing speed is set to be 4 m/s. The London road map has been transformed into the monochrome image as shown in Fig. 26.

In the taxiing phase, the environment of the scaled prototype is chosen to be a section of London surrounding Imperial College London St Mary's Campus (London W2 1PG, the UK). The origin and destination are both set to be Hyde Park (London W2 2UH, the UK), and the waypoint is set to be Warwick Avenue Cabmen's Shelter (London W9 2PT, the UK). The RRT method outputs the path searching process in Fig. 27(a), and it generates the planned path in Fig. 27(b).

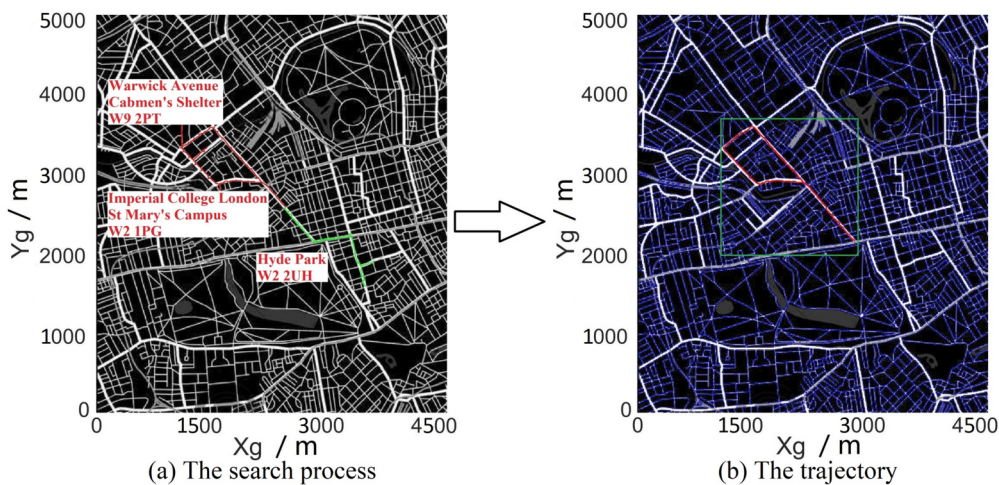


**Fig. 27.** The initial path in the taxiing phase.

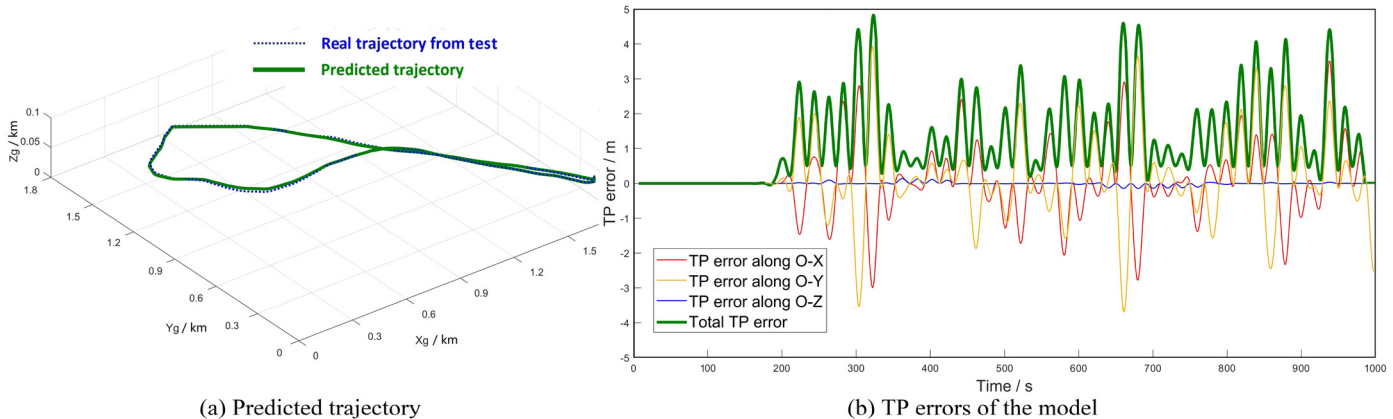


**Fig. 28.** The predicted trajectory and TP errors.

In the taxiing test, the scaled prototype moves along the initial path, and the integrated navigation system outputs the measured trajectory and full states with decimetre-level accuracy. The new TP model generates the predicted trajectory, which is compared with the test result as shown in Fig. 28(a). The TP errors of the new model are shown in Fig. 28(b).

The accuracy requirement specified at the 95th percentile is 4.544 m. To compare the new model with previous models, Equation (2) is used to calculate the total error budget for previous models, which is 35.776 m; thus, the new model has higher TP accuracy than previous models.

In the taxiing phase, the attitude errors of the new TP model are shown in Fig. 29.

The attitudes outputted by the new TP model are in conformance to the flight test results. The roll, pitch, and yaw accuracy requirements specified at the 95th percentiles are  $2.783^\circ$ ,  $1.768^\circ$ , and  $8.279^\circ$ ; thus, the total attitude accuracy requirement of the new model is  $8.911^\circ$ .

In the flight phase, the UAV prototype is constructed to a  $(1/3)$ -dimensional scale and a  $(1/3)^3$ -mass scale. The full-scale UAV has a weight of 250 kg, and its maximum load is 110 kg; thus, its total weight is 360 kg. According to dynamics similarity laws, the  $1/3$  scaled UAV prototype has a mass of 13.3333 kg. The ratio of the velocity of the scaled model to the velocity of the full-scale model is 1, and its flight speed is set to be 3 m/s. To collect the state data with decimetre-level accuracy, the UAV is equipped with a high-grade integrated GNSS/INS/LiDAR/camera navigation system. See Fig. 30.

To validate the accuracy of the navigation system, the UAV flies along a white trajectory that is pre-determined (i.e., the ground truth), and the integrated navigation system is used to measure its real-time position (i.e., the black trajectory) as shown in Fig. 31.

In the test, the position error is 0.1 m, showing that the integrated navigation system is able to output test results with decimetre-level accuracy, which can be compared with the TP model.

When the UAV flies in an urban space, it needs to avoid obstacles such as buildings; thus, the viability of the predicted trajectory is checked against the building dataset. To build an example of the realistic urban space, the representation of the buildings can be generated by using the geographic data obtained from LiDAR surveys as shown in Fig. 32.

To reduce the calculation time of the TP process, a series of cuboids and other simple shapes are generated to match and cover the boundaries of the buildings. Considering the real-world urban space, this paper sets up a corresponding UAV operational environment as shown in Fig. 33.

In the flight test, the origin and destination are stochastically determined, and then the model autonomously outputs a trajectory and waypoints (i.e., black points). The UAV autonomously flies along these waypoints (i.e., yellow points) without human control as shown in Fig. 34.

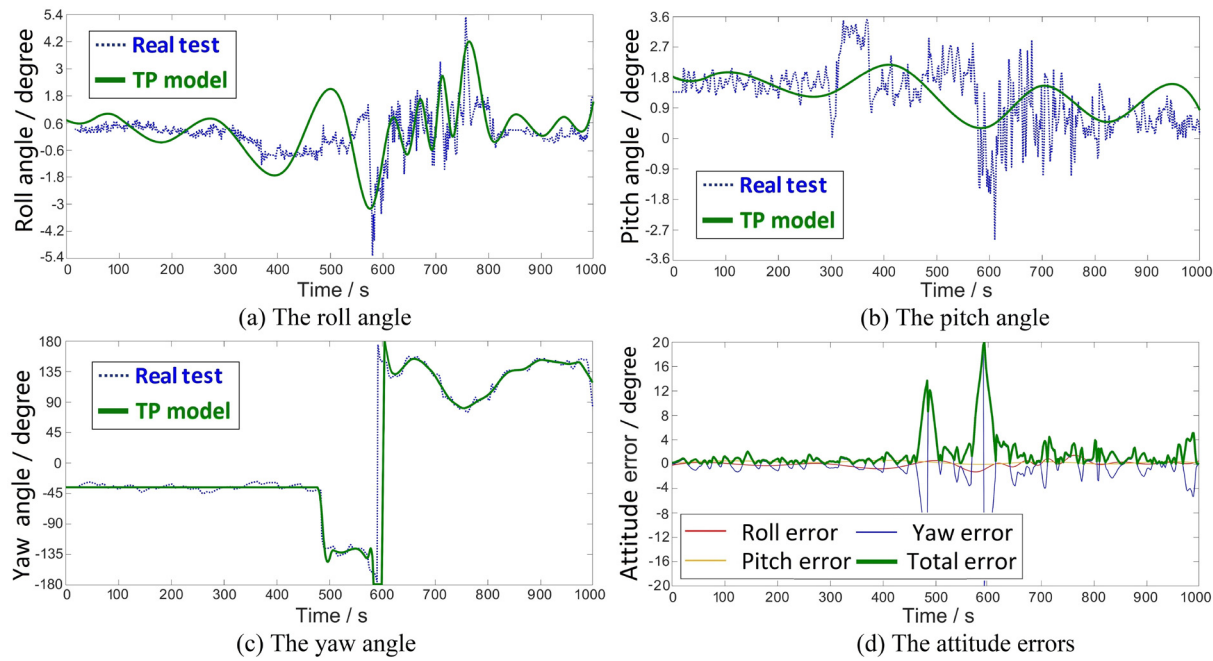


Fig. 29. The attitude errors of the TP model.



Fig. 30. Scaled UAV prototype.

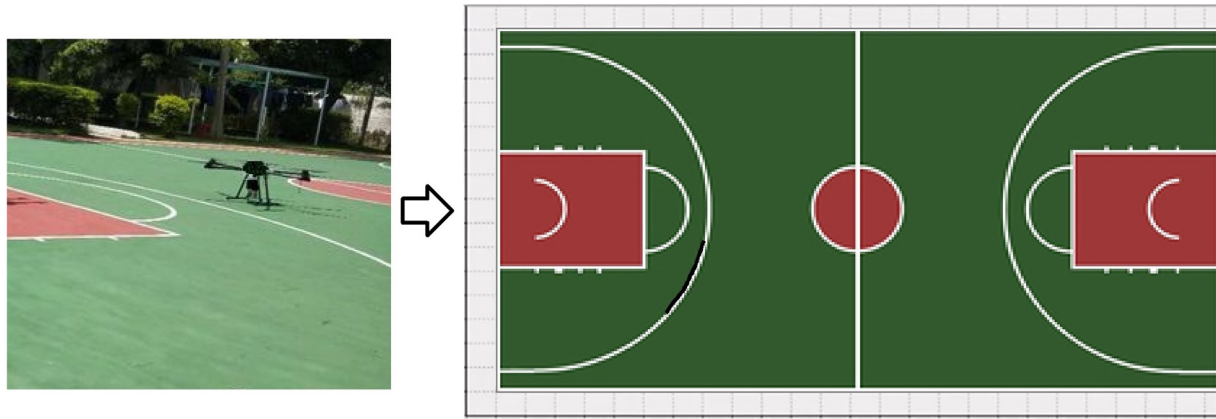


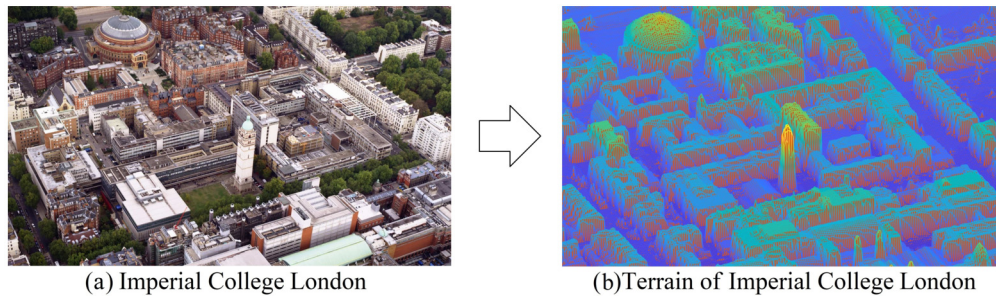
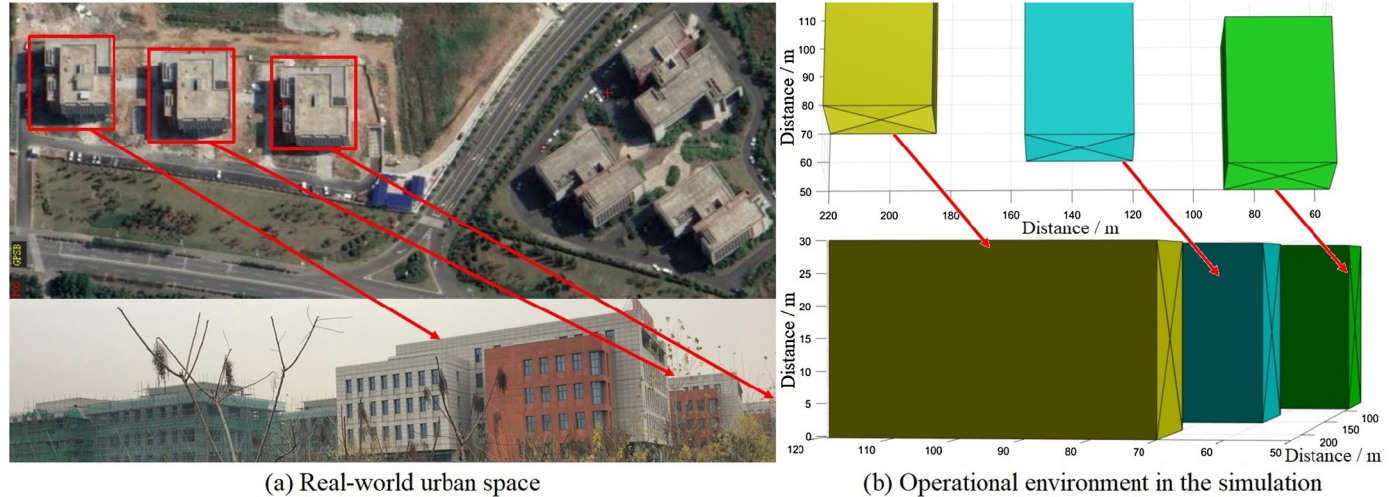
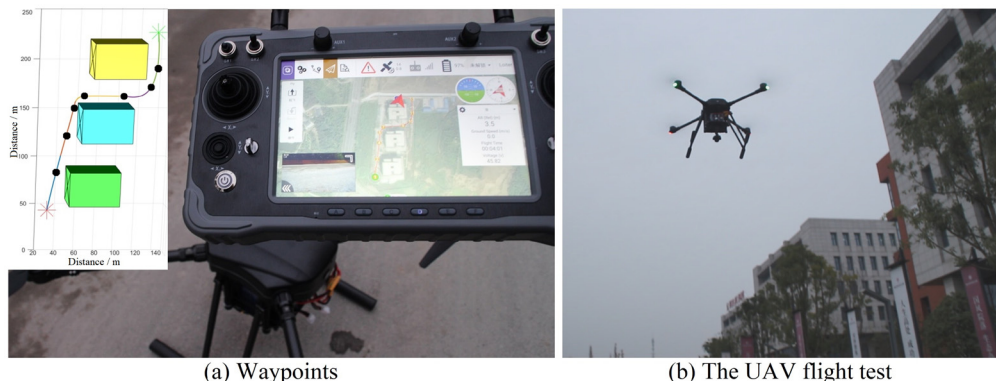
Fig. 31. Validation of the integrated navigation system.

After the flight test, the navigation system outputs the measured trajectory, which is compared with the predicted trajectories of the strategic and tactical TP models in Fig. 35.

The TP errors of the strategic and tactical models are shown in Fig. 36.

In terms of the two precedent Figures, the accuracy requirements of the strategic and tactical TP models are 6.163 m and 3.857 m. The tactical TP model has higher accuracy than the strategic TP model. To compare the new TP model with previous models, Equation (2) is used to calculate the error budget for previous models, which is 27.133 m. The new model has higher TP accuracy than previous models. The TP error along the lateral direction is evenly distributed around zero, showing that the model has high trueness along the lateral direction. The TP error along the vertical direction changes smoothly; thus, the model has high precision along the vertical direction.

In the flight phase, the attitudes of the strategic and tactical models are shown in Fig. 37.

**Fig. 32.** The detailed terrain.**Fig. 33.** Real-world urban space and its corresponding environment in simulations.**Fig. 34.** Waypoints and UAV flight tests. (For interpretation of the colours in the figure(s), the reader is referred to the web version of this article.)

The UAV attitudes outputted by the strategic and tactical TP models are in conformance to the flight test results. The attitude errors of the strategic and tactical models are shown in Fig. 38.

For the strategic TP model, the roll, pitch, and yaw accuracy requirements specified at the 95th percentiles are  $4.609^\circ$ ,  $6.791^\circ$ , and  $8.464^\circ$ ; thus, the total attitude accuracy requirement specified at the 95th percentile is  $9.908^\circ$ . For the tactical TP model, the roll, pitch, and yaw accuracy requirements specified at the 95th percentiles are  $2.616^\circ$ ,  $0.975^\circ$ , and  $6.349^\circ$ ; thus, the total attitude accuracy requirement specified at the 95th percentile is  $7.396^\circ$ . In summary, the new tactical TP model has higher attitude accuracy than the new strategic TP model.

The UAV TP error needs to be within a specified limit to enable safe en-route and terminal operations. With a 95% probability, the error needs to be within  $2\sigma_{\text{Total error}}$ . If the error exceeds this value, a warning will be issued from the UAV navigation system, directing trajectory adjustment to avoid the potential threat of flight safety.

The flight safety is linked to TP accuracy through the integrity function, which is used to monitor the TP solution. Integrity reflects the trust that can be placed in the correctness of the information supplied by the system. Specifically, when the navigation system or TP tool is unusable, it needs to deliver a warning of any malfunction (i.e., alert limit being exceeded) to users within a given period of time and with a given probability. The Alert Limit (AL) represents the largest position error allowable for safe UAV operations before causing a catastrophic problem.

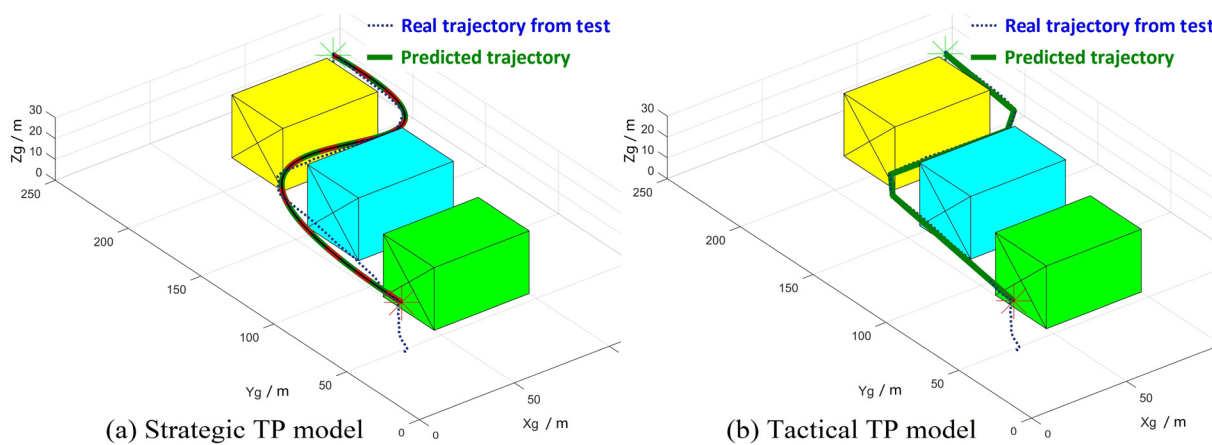


Fig. 35. The predicted trajectories of the strategic and tactical TP models.

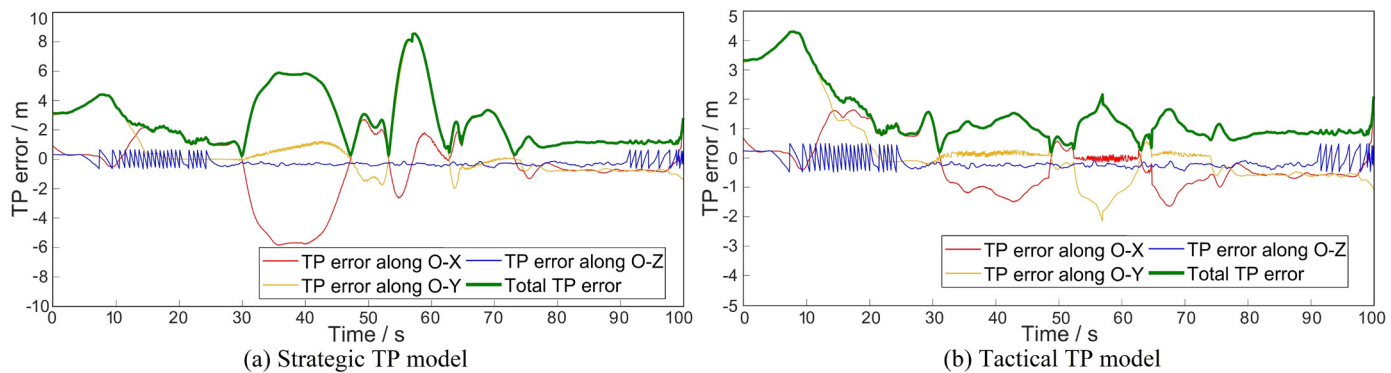


Fig. 36. The TP errors of the strategic and tactical TP models.

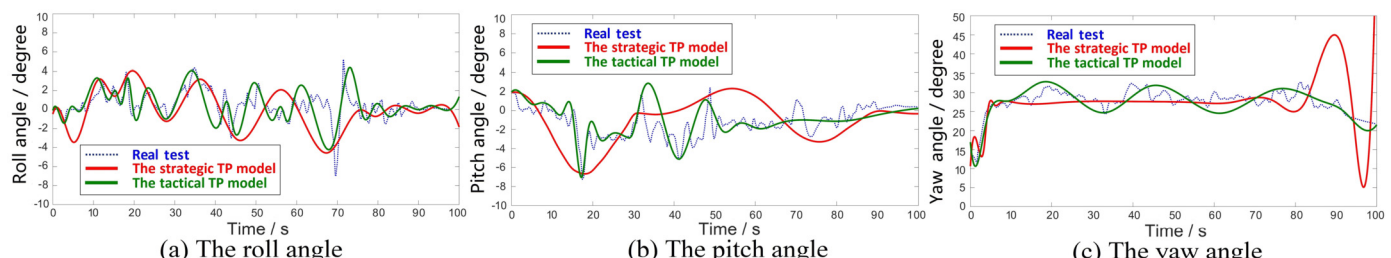


Fig. 37. The attitudes of the strategic and tactical TP models.

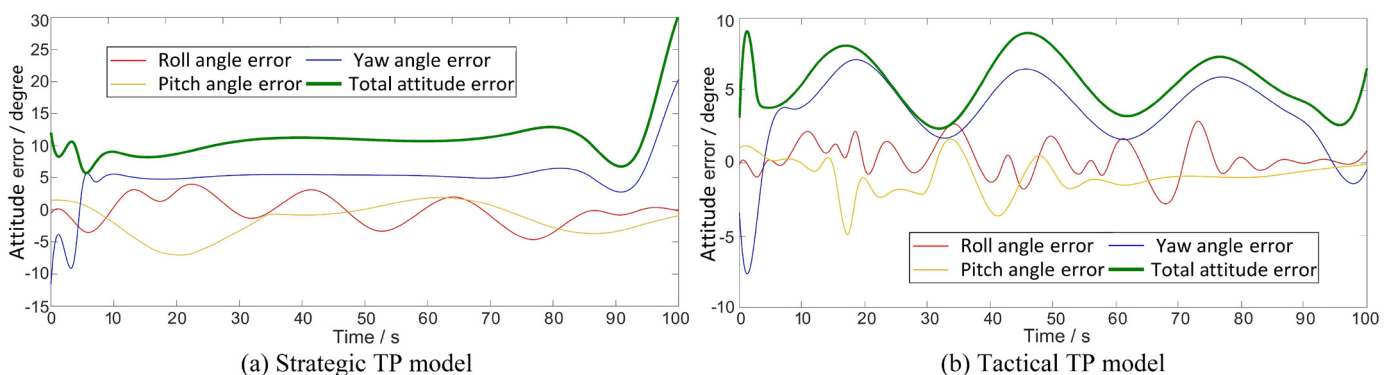


Fig. 38. The attitude errors of the strategic and tactical TP models.



**Fig. 39.** The scaled UAV prototype for real flight tests.

Compared with TP accuracy which is determined in the 95% confidence level, the AL is determined in a higher percentile confidence level to deliver integrity monitoring. If the TP model delivers errors within the expectable AL in most of the time, it is validated that the TP model has a good potential for meeting a high integrity requirement and does not need an integrity monitor necessarily; otherwise, a proper integrity monitor is required for the UAV to detect these errors to check whether they might cause failures or not.

To support UAV operations in the context of high-density urban spaces, a set of simulations and extensive tests are carried out to generate data in different flight phases to investigate the TP performance. The procedures of the tests are introduced as follows.

- The scenario is determined as the operation of the scaled passenger transport UAV in urban spaces.
- AL is determined on the basis of the simulation results, up rounded from TP errors.
- TP accuracy and AL are tested in different flight phases.
- TP errors are analysed to justify the feasibility of the proposed AL.

The integrity metrics are determined on the basis of the statistics of data, which are actual TP errors in this paper. To determine how UAVs will perform if they have integrity monitors, the sample points of the TP errors exceeding the accuracy requirement are taken into consideration. When the TP error exceeds the accuracy requirement which is specified at the 95th percentile, the stakeholders such as air traffic controllers will be told that the entire UAV system starts to fail; thus, the air traffic controllers will speak to the UAVs to increase the safety distance, which means that the system is still available even though it has a failure. When the TP error exceeds the AL for integrity monitoring, the system can no longer guarantee safety; thus, its uses must be stopped.

To test the integrity performance, the AL for integrity monitoring is specified at  $4.4\sigma_{\text{Total}}$  error (i.e., specified in the 99.999% confidence level) considering the issue on balancing the demand and safety. There might be an obstacle which is  $4.4\sigma_{\text{Total}}$  error away from the UAV; thus, the probability of the UAV position error exceeding  $4.4\sigma_{\text{Total}}$  error without alert must be less than  $10^{-5}$ , which is computed with the statistical distribution of position errors in the cross-track direction for  $4.4\sigma_{\text{Total}}$  error. If the position error of the UAV is within  $4.4\sigma_{\text{Total}}$  error at all the time, it means that the UAV is able to remain manoeuvrable, and the integrity monitor is not needed necessarily.

According to the results of the new strategic TP model, the total accuracy requirement specified at the 95th percentile is 6.163 m. The accuracy requirements in en-route and terminal phases are 7.978 m and 4.095 m. The AL is specified at  $4.4\sigma_{\text{Total}}$  error (i.e., specified in the 99.999% confidence level); thus, it is originally set to be 8.463 m for the en-route operation and 4.305 m for the terminal operation. The half-length of the diagonal line projection of the scaled UAV is 0.6 m after its rotors are folded; thus, the position error limit is 9.063 m for the en-route operation and 4.905 m for the terminal operation. To analyse the sensitivity of the studied UAV to an integrity monitor, the AL is finally set to be 10 m for the en-route operation and 5 m for the terminal operation. The terminal AL is higher than the en-route AL, because terminal UAV operations are more dangerous than en-route UAV operations considering the people and properties in take-off and landing areas.

To validate the feasibility of the AL for the studied UAV, the real flight tests are carried out as shown in Fig. 39. The UAV position data obtained by the integrated GNSS/INS/LiDAR/camera navigation system have been post-processed with the backward and forward nonlinear smoothing to be considered as the reference.

To determine whether the UAV needs an integrity monitor necessarily, the new TP model has been tested for 100 times. These 100 tests output 150000 sample points, and more than 95% of these samples are within the accuracy requirement. The other samples (less than 5%) exceeding the accuracy requirement need to be analysed.

In these 100 tests, the TP errors in three orthogonal directions are shown in Fig. 40(a). The TP performance in terms of accuracy in the whole profile is represented by the total TP errors in these 100 tests as shown in Fig. 40(b).

The test results show that all the output samples of TP errors are within the pre-determined AL (i.e., 10 m for the en-route operation, 5 m for the terminal operation); thus, it is validated that 10 m and 5 m are the proper ALs for en-route and terminal operations, respectively. The errors of the new TP model are stable; thus, the sensitivity of the new TP model to the integrity monitor is low. The UAV operation underpinned by the new TP model does not require a very sensitive integrity monitor to detect the samples beyond the accuracy requirement and less than the AL, because there is no sample beyond the AL in the tests. In summary, the UAV is able to remain manoeuvrable, and the integrity monitor is not needed necessarily.

In these 100 tests, the TP error distributions are shown in Fig. 41.

In these 100 tests, the TP error distributions are in conformance with the normal behaviour of distribution (i.e., Gaussian distribution). The test results validate that 10 m and 5 m are the proper ALs for en-route and terminal operations, respectively.

TP performance should be the same in statistical terms as the RNP, which is based on accuracy. Three valid case studies are implemented to validate that the new TP model is more accurate and has a higher level of accuracy requirement than previous models.

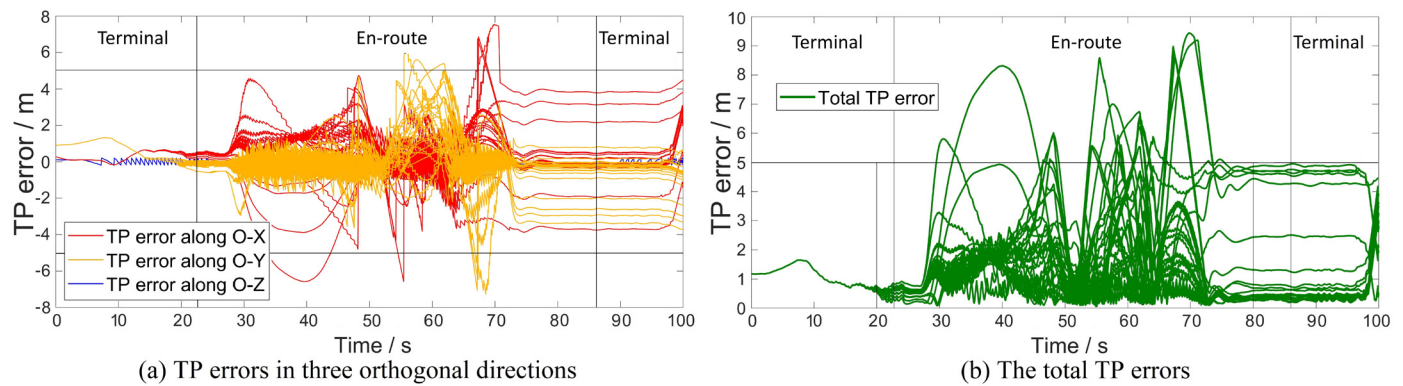


Fig. 40. TP errors in the tests.

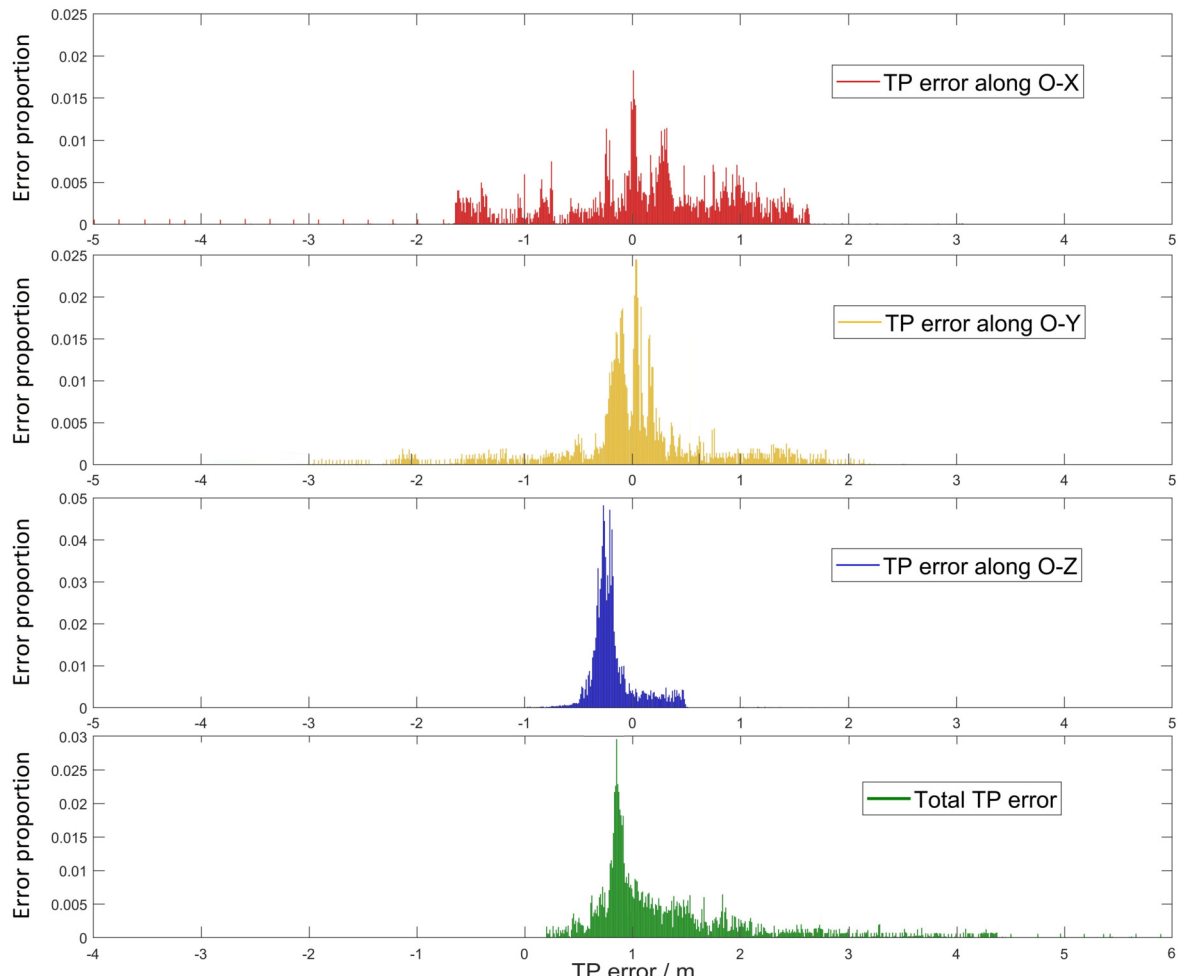


Fig. 41. TP error distributions in the tests.

## 6. Conclusions

This paper has developed a more accurate TP model by creating valid methodologies for error budgeting and mitigation. To validate and demonstrate TP accuracy in taxiing and flight phases, this paper implements three credible case studies in relation to the most stringent UAV applications (i.e., suburban logistics using HTOL UAVs, current humanitarian delivery using hybrid UAVs, and future urban passenger transport using VTOL UAVs).

In logistics, TP accuracy is 146.555 m, which is higher than previous models (i.e., 395.273 m). In humanitarian delivery, TP accuracy is 2.19 m in taxiing phases and 256.2 m in flight phases, which are both higher than previous models (i.e., 8.944 m in taxiing phases, 447 m in flight phases). In urban passenger transport, the TP accuracy requirements of the strategic and tactical models are 6.163 m and 3.857 m, which are both higher than previous models (i.e., 27.133 m). The total attitude errors of the new strategic and tactical TP models (specified at the 95th percentiles) are both less than  $10^\circ$ . The error distributions of the new TP model are in conformance to the normal behaviour of distribution (i.e., Gaussian distribution). Overall, the new model has improved TP accuracy based on previous models.

There is no model that captures the correlations between accuracy and the other RNP parameters: integrity, continuity, and availability. The work of this paper is a start of the research on the TP models covering the other RNP parameters. The improvements of these RNP parameters in the TP models shall compose the objective of our future work.

## Declaration of competing interest

The authors declare that they have no known competing financial interests or personal relationships that could have appeared to influence the work reported in this paper.

## References

- [1] D. Floreano, R.J. Wood, Science, technology and the future of small autonomous drones, *Nature* 521 (7553) (2015) 460–466, <https://doi.org/10.1038/nature14542>.
- [2] G.D. Goh, S. Agarwala, G.L. Goh, V. Dikshit, S.L. Sing, W.Y. Yeong, Additive manufacturing in unmanned aerial vehicles (UAVs): challenges and potential, *Aerosp. Sci. Technol.* 63 (2017) 140–151, <https://doi.org/10.1016/j.ast.2016.12.019>.
- [3] J. Park, H. Baek, Stereo vision based obstacle collision avoidance for a quadrotor using ellipsoidal bounding box and hierarchical clustering, *Aerosp. Sci. Technol.* 103 (2020) 105882, <https://doi.org/10.1016/j.ast.2020.105882>.
- [4] Y. Song, L. Hsu, Tightly coupled integrated navigation system via factor graph for UAV indoor localization, *Aerosp. Sci. Technol.* 108 (2021) 106370, <https://doi.org/10.1016/j.ast.2020.106370>.
- [5] T. Tomic, K. Schmid, P. Lutz, A. Domel, M. Kassecker, E. Mair, I. Grix, F. Ruess, M. Suppa, D. Burschka, Toward a fully autonomous UAV: research platform for indoor and outdoor urban search and rescue, *IEEE Robot. Autom. Mag.* 19 (2012) 46–56, <https://doi.org/10.1109/MRA.2012.2206473>.
- [6] X. He, J. Montillet, R. Fernandes, M. Bos, K. Yu, X. Hua, W. Jiang, Review of current GPS methodologies for producing accurate time series and their error sources, *J. Geodyn.* 106 (2017) 12–29, <https://doi.org/10.1016/j.jog.2017.01.004>.
- [7] W.Y. Ochieng, K. Sauer, Urban road transport navigation: performance of the global positioning system after selective availability, *Transp. Res., Part C, Emerg. Technol.* 10 (2002) 171–187, [https://doi.org/10.1016/S0968-090X\(02\)00008-6](https://doi.org/10.1016/S0968-090X(02)00008-6).
- [8] W.Y. Ochieng, K. Sauer, D. Walsh, G. Brodin, S. Griffin, M. Denney, GPS integrity and potential impact on aviation safety, *J. Navig.* 56 (2003) 51–65, <https://doi.org/10.1017/s0373463302002096>.
- [9] C. Magaña, E. Juan, Trajectory prediction uncertainty modelling for Air Traffic Management, University of Glasgow, 2016, pp. 1–254, <http://theses.gla.ac.uk/7700/>.
- [10] R. Alligier, D. Gianazza, N. Durand, Machine learning and mass estimation methods for ground-based aircraft climb prediction, *IEEE Trans. Intell. Transp. Syst.* 16 (2015) 3138–3149, <https://doi.org/10.1109/TITS.2015.2437452>.
- [11] J. Sun, J. Ellerbroek, J.M. Hoekstra, Aircraft initial mass estimation using Bayesian inference method, *Transp. Res., Part C, Emerg. Technol.* 90 (2018) 59–73, <https://doi.org/10.1016/j.trc.2018.02.022>.
- [12] J. Sun, H. Blom, J. Ellerbroek, J.M. Hoekstra, Particle filter for aircraft mass estimation and uncertainty modeling, *Transp. Res., Part C, Emerg. Technol.* 105 (2019) 145–462, <https://doi.org/10.1016/j.trc.2019.05.030>.
- [13] R. Alligier, D. Gianazza, Learning aircraft operational factors to improve aircraft climb prediction: a large scale multi-airport study, *Transp. Res., Part C, Emerg. Technol.* 96 (2018) 72–95, <https://doi.org/10.1016/j.trc.2018.08.012>.
- [14] Y.S. Chati, B. Hamsa, Modeling of aircraft takeoff weight using Gaussian processes, *Air Traffic Control Q.* 26 (2018) 70–79, <https://doi.org/10.2514/1.d0099>.
- [15] J. Zhang, J. Liu, R. Hu, H. Zhu, Online four dimensional trajectory prediction method based on aircraft intent updating, *Aerosp. Sci. Technol.* 77 (2018) 774–787, <https://doi.org/10.1016/j.ast.2018.03.037>.
- [16] R. Chai, A. Savvaris, A. Tsourdos, Y. Xia, Unified multiobjective optimization scheme for aeroassisted vehicle trajectory planning, *J. Guid. Control Dyn.* 41 (2018) 1521–1530, <https://arc.aiaa.org/doi/10.2514/1.G003189>.
- [17] R. Chai, A. Savvaris, A. Tsourdos, S. Chai, Solving trajectory optimization problems in the presence of probabilistic constraints, *IEEE Trans. Cybern.* 50 (2020) 1–14, <https://doi.org/10.1109/TCYB.2019.2895305>.
- [18] R. Chai, A. Savvaris, A. Tsourdos, S. Chai, Fast generation of chance-constrained flight trajectory for unmanned vehicles, *IEEE Trans. Aerosp. Electron. Syst.* 11 (2020) 1028–1045, <https://doi.org/10.1109/TAES.2020.3037417>.
- [19] Y. Liu, H. Wang, Z. Su, J. Fan, Deep learning based trajectory optimization for UAV aerial refuelling docking under bow wave, *Aerosp. Sci. Technol.* 80 (2018) 392–402, <https://doi.org/10.1016/j.ast.2018.07.024>.
- [20] R. Chai, A. Tsourdos, A. Savvaris, S. Chai, Design and implementation of deep neural network-based control for automatic parking maneuver process, *IEEE Trans. Neural Netw. Learn. Syst.* 99 (2020) 1–14, <https://doi.org/10.1109/TNNLS.2020.3042120>.
- [21] R. Chai, A. Tsourdos, A. Savvaris, S. Chai, Six-DOF spacecraft optimal trajectory planning and real-time attitude control: a deep neural network-based approach, *IEEE Trans. Neural Netw. Learn. Syst.* 12 (2019) 5005–5013, <https://doi.org/10.1109/TNNLS.2019.2955400>.
- [22] F. Causa, G. Fasano, Multiple UAVs trajectory generation and waypoint assignment in urban environment based on DOP maps, *Aerosp. Sci. Technol.* 110 (2021) 106507, <https://doi.org/10.1016/j.ast.2021.106507>.
- [23] Y. Liu, H. Wang, J. Fan, J. Wu, T. Wu, Control-oriented UAV highly feasible trajectory planning: a deep learning method, *Aerosp. Sci. Technol.* 110 (2021) 106435, <https://doi.org/10.1016/j.ast.2020.106435>.
- [24] A. Renault, A model for assessing UAV system architectures, *Proc. Comput. Sci.* 61 (2015) 160–167, <https://doi.org/10.1016/j.procs.2015.09.180>.
- [25] M. Hassanalian, A. Abdelkefi, Classifications, applications, and design challenges of drones: a review, *Prog. Aerosp. Sci.* 91 (2017) 99–131, <https://doi.org/10.1016/j.paerosci.2017.04.003>.
- [26] M. Alwateer, S.W. Loke, A.M. Zuchowicz, Drone services: issues in drones for location-based services from human-drone interaction to information processing, *J. Locat. Based Serv.* 13 (2019) 1–34, <https://doi.org/10.1080/17489725.2018.1564845>.
- [27] Y. Hauss, K. Eyerth, Securing future ATM-concepts' safety by measuring situation awareness in ATC, *Aerosp. Sci. Technol.* 6 (2003) 417–427, [https://doi.org/10.1016/S1270-9638\(02\)00011-1](https://doi.org/10.1016/S1270-9638(02)00011-1).
- [28] L. Yin, Q. Ni, Z. Deng, A GNSS/5G integrated positioning methodology in D2D communication networks, *IEEE J. Sel. Areas Commun.* 36 (2018) 351–362, <https://doi.org/10.1109/J SAC.2018.2804223>.
- [29] A.R. Merheb, H. Noura, F. Bateman, Emergency control of AR drone quadrotor UAV suffering a total loss of one rotor, *IEEE/ASME Trans. Mechatron.* 22 (2017) 961–971, <https://doi.org/10.1109/TMECH.2017.2652399>.
- [30] S. Chang, A. Cho, S. Choi, Y. Kang, Y. Kim, M. Kim, Flight testing full conversion of a 40-kg-class tilt-duct unmanned aerial vehicle, *Aerosp. Sci. Technol.* 112 (2021) 106611, <https://doi.org/10.1016/j.ast.2021.106611>.
- [31] H. Georgiou, N. Pelekis, S. Sideridis, D. Scarlatti, Y. Theodoridis, Semantic-aware aircraft trajectory prediction using flight plans, *Int. J. Data Sci. Anal.* 9 (2020) 215–228, <https://doi.org/10.1007/s41060-019-00182-4>.
- [32] M. Hassanalian, R. Salazar, A. Abdelkefi, Conceptual design and optimization of a tilt-rotor micro air vehicle, *Chin. J. Aeronaut.* 32 (2019) 159–171, <https://CNKI:SUN:HKXS.0.2019-02-013>.
- [33] M. Xue, UAV trajectory modeling using neural networks, in: *17th AIAA Aviat. Integr. Oper.*, vol. 6, 2017, pp. 1–10.
- [34] Z. Zhang, R. Du, R.V. Cowlagi, Randomized sampling-based trajectory optimization for UAVs to satisfy linear temporal logic specifications, *Aerosp. Sci. Technol.* 96 (2019) 105591, <https://doi.org/10.1016/j.ast.2019.105591>.
- [35] J.E. Macias, P. Angeloudis, W.Y. Ochieng, Optimal hub selection for rapid medical deliveries using unmanned aerial vehicles, *Transp. Res., Part C, Emerg. Technol.* 110 (2020) 56–80, <https://doi.org/10.1016/j.trc.2019.11.002>.
- [36] J.E. Macias, N. Goldbeck, P.Y. Hsu, P. Angeloudis, W.Y. Ochieng, Endogenous stochastic optimisation for relief distribution assisted with unmanned aerial vehicles, *OR Spectrum* 42 (2020) 1089–1125, <https://doi.org/10.1007/s00291-020-00602-z>.
- [37] F. Favoino, E. Raheli, D. Ramirez, F. Pilosio, S. Tavernese, M. Simonetti, M. Perino, M. Masoero, Impact of glass technology on future electrical individual transportation: the Pop.Up case study, *Glass. Struct. Eng.* 5 (2020) 117–131, <https://doi.org/10.1007/s40940-019-00104-7>.